

Thermoelectric transport and current noise through a multilevel Anderson impurity: Three-body Fermi-liquid corrections in quantum dots and magnetic alloys

Yoshimichi Teratani,^{1,2} Kazuhiko Tsutsumi,^{1,2} Kaiji Motoyama,^{1,3} Rui Sakano,⁴ and Akira Oguri^{1,2}

¹*Department of Physics, Osaka City University, Sumiyoshi-ku, Osaka 558-8585, Japan*

²*Nambu Yoichiro Institute of Theoretical and Experimental Physics,
Osaka Metropolitan University, Osaka 558-8585, Japan*

³*Department of Physics, Osaka Metropolitan University, Sumiyoshi-ku, Osaka 558-8585, Japan*

⁴*Department of Physics, Keio University, 3-14-1 Hiyoshi,
Kohoku-ku, Yokohama, Kanagawa 223-8522, Japan*

(Dated: November 12, 2024)

We present a comprehensive Fermi liquid description for thermoelectric transport and current noise, applicable to multilevel quantum dots (QD) and magnetic alloys (MA) without electron-hole or time-reversal symmetry. Our formulation for the low-energy transport is based on an Anderson model with N discrete impurity levels, and is asymptotically exact at low energies, up to the next-leading order terms in power expansions with respect to temperature T and bias voltage eV . The expansion coefficients can be expressed in terms of the Fermi liquid parameters, which include the three-body correlation functions defined with respect to the equilibrium ground state in addition to the linear susceptibilities and the occupation number N_d of impurity electrons. We apply this formulation to the $SU(N)$ symmetric QD and MA, and calculate the correlation functions for $N = 4$ and 6, using numerical renormalization group approach. The three-body correlations are shown to be determined by a single parameter over a wide range of electron fillings $1 \lesssim N_d \lesssim N - 1$ for strong Coulomb interactions U , and they also exhibit the plateau structures due to the $SU(N)$ Kondo effects at integer values of N_d . We find that the Lorenz number $L = \kappa/(T\sigma)$ for QD and MA, defined as the ratio of the thermal conductivity κ to the electrical conductivity σ , deviates from the universal Wiedemann-Franz value $\pi^2/(3e^2)$ as the temperature increases from $T = 0$, showing the T^2 dependence, the coefficient for which depends on the three-body correlations away from half filling. Furthermore, we find that the current noise for the $SU(4)$ quantum dots and that for $SU(6)$ show a pronounced difference at the quarter $N_d/N = 1/4$ and $3/4$ fillings. In particular, the linear noise for $N = 4$ exhibits a flat peak while the peak for $N = 6$ shows a round shape, reflecting the fact that, at these filling points, the $SU(N)$ Kondo effects occur for $N \equiv 0 \pmod{4}$, whereas the intermediate-valence fluctuations occur for $N \equiv 2 \pmod{4}$. We also demonstrate the role of three-body correlations on the nonlinear current noise and the other transport coefficients.

PACS numbers: 71.10.Ay, 71.27.+a, 72.15.Qm

I. INTRODUCTION

The Kondo effect is a fascinating many-body effect [1, 2], taking place in dilute magnetic alloys (MA), quantum dots (QD), and other novel quantum systems such as ultracold atomic gases [3] and quark matter [4]. It was shown in the 1970s that the low-energy behavior of the Kondo systems can be described by a quantum impurity version of the Fermi liquid (FL) theory [5–9]. In particular, using the numerical renormalization group (NRG) approach [10–12], Wilson *et al.* demonstrated that the low-lying excited states of the Kondo and the Anderson models exhibit a one-to-one correspondence with the excitations of the renormalized quasiparticles.

The quasiparticles are asymptotically free in the equilibrium ground state, where the perturbations from the environment or reservoirs, which may depend on external parameters such as frequency ω , temperature T , bias voltages eV , etc., are absent. As these perturbations are adiabatically switched on, the quasiparticles capture the damping rate of order ω^2 , T^2 , and $(eV)^2$ through the residual interactions and this significantly affects the transport properties [5–9, 13, 14]. When the electron-

hole or time-reversal symmetry is broken by a potential or external fields, the quasiparticles also capture the energy shift of order ω^2 , T^2 , and $(eV)^2$, i.e., the corrections in the same order as the ones due to the damping rate. The contributions of these higher-order energy shifts, however, had not been fully understood until very recently.

It has recently been clarified that these higher-order energy shifts of the quasiparticles can be described exactly in terms of the three-body correlations between impurity electrons. The proof was given in two different ways, which complement each other. One is given by Mora *et al.* and Filippone *et al.* [15–18], extending Nozières’ description [5] that is based on an invariance against the “floating of Kondo resonance on the Fermi sea”. The other is based on the higher-order Fermi liquid relations [19–21], which can be derived from the Ward identities for the second derivatives of the self-energy, extending Yamada-Yosida’s field-theoretical approach [6–9]. These proofs enabled one to express the next-leading order terms of the transport coefficients in terms of three-body correlation functions, and these formulations have been applied to the nonlinear currents, current noise,

and thermocurrent through quantum impurities without electron-hole or time-reversal symmetry [22–29].

The purpose of this paper is twofold. The first one is to extend the latest version of the FL theory for treating the thermoelectric transport coefficients of multilevel quantum dots and magnetic alloys described by the Anderson model with N arbitrary impurity levels. The second one is to demonstrate how the next-leading order terms of various transport coefficients vary with the impurity level ϵ_d and Coulomb interaction U . Specifically, for the second purpose, we consider quantum dots and magnetic alloys having an $SU(N)$ symmetry, and calculate the three-body correlation functions for $N = 4$ and 6 using the NRG approach. There have been a number of intensive works which theoretically studied low-energy transport: the nonlinear current [13, 14, 18, 30–37], nonlinear current noise [16, 23, 38–42], and thermoelectric transport [15, 21, 43, 44]. However, the parameter space for quantum impurities is so huge that many parts are still left unexplored. In this paper, we explore the whole region of the electron fillings, $0 \leq N_d \leq N$, in which the occupation number N_d of electrons in the impurity levels varies continuously across the various $SU(N)$ Kondo and intermediate valence regimes.

One of the advantages of the Kondo systems realized in quantum dots is that the information about the many-body quantum states can be probed in such a highly tunable way [45–48]. For instance, recent experiments have succeeded in directly probing the Kondo screening cloud [49]. Furthermore, low-energy Fermi liquid behaviors have experimentally been confirmed for nonequilibrium currents [50, 51], current noise [52–56], and thermocurrent [57, 58]. Internal degrees of freedoms of quantum impurities also bring an interesting variety to the Kondo effect. The systems having the $SU(4)$ symmetry have been realized, for instance, in the multiorbital semiconductor quantum dots and carbon nanotube (CNT) quantum dots [59], and have intensively been investigated theoretically [15, 16, 22, 26, 34, 60–68] and experimentally [55, 69–73]. Realization of the $SU(N)$ Kondo effects for various $N > 2$ has also been proposed by several authors, using triple quantum dots [74, 75] and CNT [76]. In this paper, we provide a comprehensive FL view of the low-energy transport for $SU(4)$ and $SU(6)$ symmetric QD and MA.

Our results reveal the fact that the three-body correlations exhibit plateau structures, caused by the $SU(N)$ Kondo effects occurring at integer fillings $N_d = 1, 2, \dots, N - 1$. We also calculate the Lorenz number $L = \kappa/(T\sigma)$ for QD and MA, defined as the ratio of the thermal conductivity κ to the electrical conductivity σ , and show how it deviates from the universal Wiedemann-Franz value $\pi^2/(3e^2)$ as the temperature increases from $T = 0$. Furthermore, we demonstrate how the three-body correlations affect the order T^2 electrical conductivity, the order T^3 thermal conductivity, and the order $(eV)^3$ nonlinear current and current noise. At quarter $N_d/N = 1/4$ and three-quarters $N_d/N = 3/4$ fillings, the

$SU(N)$ Kondo effects occur for $N \equiv 0 \pmod{4}$ while the intermediate valence fluctuations occur for $N \equiv 2 \pmod{4}$. We show that this dependence on $(\text{mod } 4)$ causes a pronounced difference appearing in the peak structures of linear noise for $N = 4$ and 6.

This paper is organized as follows. In Sec. II, we describe the multilevel Anderson impurity model for quantum dots and magnetic alloys. Sections III and IV are devoted to the FL descriptions for the next-leading order terms of electrical and thermoelectric transport coefficients for quantum dots, applicable to arbitrary N impurity-level structures. In Sec. V, the low-energy transport formulas for the $SU(N)$ quantum dots are described in terms of the five FL parameters. We present the NRG results for the three-body correlation functions in Sec. VI. The results for nonlinear current, current noise, and thermoelectric transport through quantum dots are discussed in Secs. VII and VIII. Section IX is devoted to the FL description of the three-body correlations in thermoelectric transport of dilute magnetic alloys. In Sec. X, we discuss the results for the electrical and thermal resistivities of the $SU(4)$ and $SU(6)$ magnetic alloys. Summary is given in Sec. XI. In Appendix, we provide details of the derivations for the transport formulas and additional NRG results for the FL parameters in the $SU(N)$ cases for $N = 2, 4$, and 6, for comparison.

II. MODEL

We consider a multi-orbital Anderson impurity coupled to two noninteracting leads on the left (L) and right (R): $\mathcal{H} = \mathcal{H}_d + \mathcal{H}_c + \mathcal{H}_T$,

$$\mathcal{H}_d = \sum_{\sigma=1}^N \epsilon_{d\sigma} n_{d\sigma} + \frac{1}{2} \sum_{\sigma \neq \sigma'} U_{\sigma\sigma'} n_{d\sigma} n_{d\sigma'}, \quad (2.1)$$

$$\mathcal{H}_c = \sum_{j=L,R} \sum_{\sigma=1}^N \int_{-D}^D d\epsilon \epsilon c_{\epsilon j\sigma}^\dagger c_{\epsilon j\sigma}, \quad (2.2)$$

$$\mathcal{H}_T = - \sum_{j=L,R} \sum_{\sigma=1}^N v_j \left(\psi_{j,\sigma}^\dagger d_\sigma + d_\sigma^\dagger \psi_{j,\sigma} \right). \quad (2.3)$$

Here, the level index runs over $\sigma = 1, 2, \dots, N$. The inter-electron interaction $U_{\sigma\sigma'}$ generally depends on σ and σ' , with the requirements $U_{\sigma'\sigma} = U_{\sigma\sigma'}$, for $\sigma' \neq \sigma$. For $N = 2$, it describes the usual single-orbital Anderson model for spin 1/2 fermions. The operator d_σ^\dagger creates an impurity electron with spin σ in the impurity level of energy $\epsilon_{d\sigma}$, and $n_{d\sigma} \equiv d_\sigma^\dagger d_\sigma$. Conduction electrons in the two lead at $j = L$ and R obey the anti-commutation relation $\{c_{\epsilon j\sigma}, c_{\epsilon' j'\sigma'}^\dagger\} = \delta_{jj'} \delta_{\sigma\sigma'} \delta(\epsilon - \epsilon')$. The linear combination of the conduction electrons, $\psi_{j,\sigma} \equiv \int_{-D}^D d\epsilon \sqrt{\rho_c} c_{\epsilon j\sigma}$ with $\rho_c = 1/(2D)$, couples to the impurity level. The bare level width due to the tunnel couplings is given by $\Delta \equiv \Gamma_L + \Gamma_R$ with $\Gamma_j = \pi \rho_c v_j^2$. We consider the parameter region where the half band-width D is much greater than

the other energy scales, $D \gg \max(U_{\sigma\sigma'}, \Delta, |\epsilon_{d\sigma}|, T, |eV|)$. We use a unit $k_B = 1$ throughout this paper.

Low-energy properties of the Anderson model can be described in terms of a set of Fermi liquid parameters defined with respect to the equilibrium ground state, i.e., the phase shift δ_σ , the linear susceptibilities $\chi_{\sigma\sigma'}$ and the three-body correlation functions $\chi_{\sigma\sigma'\sigma''}^{[3]}$ between impurity electrons; see Appendix A for details. The phase shift is a primary parameter that reflects the charge distribution of impurity levels, through the Friedel sum rule: $\langle n_{d\sigma} \rangle \xrightarrow{T \rightarrow 0} \delta_\sigma/\pi$. In this paper, we explore the low-energy transport of quantum dots and magnetic alloys in the whole region of the electron fillings,

$$N_d \equiv \sum_{\sigma=1}^N \langle n_{d\sigma} \rangle. \quad (2.4)$$

The current conservation, which follows from the Heisenberg equation of motion for the occupation number $n_{d\sigma}$,

$$\frac{\partial n_{d\sigma}}{\partial t} + \hat{J}_{R,\sigma} - \hat{J}_{L,\sigma} = 0 \quad (2.5)$$

also plays an essential role in the Fermi liquid description, through the Ward identities. Here, $\hat{J}_{L,\sigma}$ represents the current flowing from the left lead to the dot, and $\hat{J}_{R,\sigma}$ the current from the dot to the right lead:

$$\hat{J}_{L,\sigma} = -i v_L \left(\psi_{L\sigma}^\dagger d_\sigma - d_\sigma^\dagger \psi_{L\sigma} \right), \quad (2.6)$$

$$\hat{J}_{R,\sigma} = +i v_R \left(\psi_{R\sigma}^\dagger d_\sigma - d_\sigma^\dagger \psi_{R\sigma} \right). \quad (2.7)$$

In the next section, we will give a brief overview of the low-energy expansion formulas for nonlinear current and current noise, obtained previously in Refs. 27 and 29, to show how the formulas can be expressed in terms of the FL parameters, including the three-body correlations. This is for comparison with the formulas for thermal electric transport coefficients, which we extend to multilevel quantum dots and magnetic alloys in this paper. Specifically, we will describe the derivation of the formulas for multilevel quantum dots and magnetic alloys in Sec. IV and Appendix G, respectively.

III. FERMI LIQUID DESCRIPTION FOR NONLINEAR CURRENT NOISE OF QD

We consider the nonequilibrium steady state under a finite bias voltage $eV \equiv \mu_L - \mu_R$, applied between the two leads by setting the chemical potentials of the left and right leads to be μ_L and μ_R , respectively. The retarded Green's function plays a central role in the microscopic description of the Fermi liquid transport:

$$G_\sigma^r(\omega) = -i \int_0^\infty dt e^{i(\omega+i0^+)t} \left\langle \left\{ d_\sigma(t), d_\sigma^\dagger \right\} \right\rangle_V, \quad (3.1)$$

$$A_\sigma(\omega) \equiv -\frac{1}{\pi} \text{Im} G_\sigma^r(\omega). \quad (3.2)$$

Here, $\langle \dots \rangle_V$ represents a nonequilibrium steady-state average taken with the statistical density matrix, which is constructed at finite bias voltages eV and temperatures T , using the Keldysh formalism [13, 33, 77].

A. Differential conductance dJ/dV

The nonequilibrium current J through quantum dots can be expressed in terms of the spectral function $A_\sigma(\omega)$ [13, 33]:

$$J = \frac{e}{h} \sum_\sigma \int_{-\infty}^\infty d\omega [f_L(\omega) - f_R(\omega)] \mathcal{T}_\sigma(\omega), \quad (3.3)$$

$$\mathcal{T}_\sigma(\omega) = \frac{4\Gamma_L\Gamma_R}{\Gamma_L + \Gamma_R} \pi A_\sigma(\omega). \quad (3.4)$$

Here, $f_j(\omega) \equiv f(\omega - \mu_j)$ for $j = L, R$, with $f(\omega) = [e^{\omega/T} + 1]^{-1}$ the Fermi function. Specifically, in this paper, we consider the case where the chemical potentials are applied in a symmetric way:

$$\mu_L = -\mu_R \equiv \frac{1}{2} eV, \quad (3.5)$$

choosing the Fermi level at equilibrium to be the origin of one-particle energies $E_F = 0$. Note that the role of bias and tunneling asymmetries, $(\mu_L + \mu_R)/2 \neq E_F$ and $\Gamma_L \neq \Gamma_R$, has been precisely discussed in Refs. 28 and 29.

The nonlinear current J can be expanded up to the next-leading order terms, using the low-energy asymptotic form of the spectral function $A_\sigma(\omega)$, which has been obtained up to terms of order ω^2 , $(eV)^2$, and T^2 [27], as shown in Appendix B. In particular, for symmetric junctions with $\Gamma_L = \Gamma_R$ and $\mu_L = -\mu_R = eV/2$, the low-energy expansion of the differential conductance takes the form,

$$\frac{dJ}{dV} = \frac{e^2}{h} \sum_{\sigma=1}^N \left[\sin^2 \delta_\sigma - c_{T,\sigma} (\pi T)^2 - c_{V,\sigma} (eV)^2 + \dots \right]. \quad (3.6)$$

Here, the coefficients $c_{T,\sigma}$ and $c_{V,\sigma}$ of the next-leading order terms can be expressed in terms of the phase shift δ_σ , the linear susceptibilities $\chi_{\sigma\sigma'}$, and the static three-body correlation functions $\chi_{\sigma\sigma'\sigma''}^{[3]}$ defined in Appendix

A:

$$c_{T,\sigma} = \frac{\pi^2}{3} \left[- \left(\chi_{\sigma\sigma}^2 + 2 \sum_{\sigma'(\neq\sigma)} \chi_{\sigma\sigma'}^2 \right) \cos 2\delta_\sigma + \left(\chi_{\sigma\sigma\sigma}^{[3]} + \sum_{\sigma'(\neq\sigma)} \chi_{\sigma\sigma'\sigma'}^{[3]} \right) \frac{\sin 2\delta_\sigma}{2\pi} \right], \quad (3.7)$$

$$c_{V,\sigma} = \frac{\pi^2}{4} \left[- \left(\chi_{\sigma\sigma}^2 + 5 \sum_{\sigma'(\neq\sigma)} \chi_{\sigma\sigma'}^2 \right) \cos 2\delta_\sigma + \left(\chi_{\sigma\sigma\sigma}^{[3]} + 3 \sum_{\sigma'(\neq\sigma)} \chi_{\sigma\sigma'\sigma'}^{[3]} \right) \frac{\sin 2\delta_\sigma}{2\pi} \right]. \quad (3.8)$$

B. Nonlinear current noise $S_{\text{noise}}^{\text{QD}}$

We also study the current noise [26, 27, 78], defined by

$$S_{\text{noise}}^{\text{QD}} = e^2 \sum_{\sigma\sigma'} \int_{-\infty}^{\infty} dt \left\langle \delta \hat{J}_\sigma(t) \delta \hat{J}_{\sigma'}(0) + \delta \hat{J}_{\sigma'}(0) \delta \hat{J}_\sigma(t) \right\rangle_V. \quad (3.9)$$

Here, $\delta \hat{J}_\sigma(t) \equiv \hat{J}_\sigma(t) - \langle \hat{J}_\sigma(0) \rangle_V$ represents fluctuations of the symmetrized current:

$$\hat{J}_\sigma \equiv \frac{\Gamma_L \hat{J}_{R,\sigma} + \Gamma_R \hat{J}_{L,\sigma}}{\Gamma_L + \Gamma_R}. \quad (3.10)$$

Behavior of the current noise in the low-energy Fermi liquid regime has been studied by several authors, taking into account the three-body correlations [16, 17]. In a previous work, we have derived a general formula for the current noise through the multilevel Anderson impurity model up to terms of order $|eV|^3$ for symmetric junctions $\Gamma_L = \Gamma_R$ and $\mu_L = -\mu_R = eV/2$ [26, 27]:

$$S_{\text{noise}}^{\text{QD}} = \frac{2e^2}{h} |eV| \sum_{\sigma=1}^N \left[\frac{\sin^2 2\delta_\sigma}{4} + c_{S,\sigma} (eV)^2 + \dots \right]. \quad (3.11)$$

The coefficient $c_{S,\sigma}$ for the next-leading order term has been calculated by taking into account all components of the Keldysh vertex function together with the low-energy asymptotic form of $A_\sigma(\omega)$. It has been shown to be expressed in the following form,

$$c_{S,\sigma} = \frac{\pi^2}{12} \left[\cos 4\delta_\sigma \chi_{\sigma\sigma}^2 + (2 + 3 \cos 4\delta_\sigma) \sum_{\sigma'(\neq\sigma)} \chi_{\sigma\sigma'}^2 + 4 \sum_{\sigma'(\neq\sigma)} \cos 2\delta_\sigma \cos 2\delta_{\sigma'} \chi_{\sigma\sigma'}^2 + 3 \sum_{\sigma'(\neq\sigma)} \sum_{\sigma''(\neq\sigma,\sigma')} \sin 2\delta_\sigma \sin 2\delta_{\sigma'} \chi_{\sigma\sigma''} \chi_{\sigma'\sigma''} - \left(\chi_{\sigma\sigma\sigma}^{[3]} + 3 \sum_{\sigma'(\neq\sigma)} \chi_{\sigma\sigma'\sigma'}^{[3]} \right) \frac{\sin 4\delta_\sigma}{4\pi} \right]. \quad (3.12)$$

IV. FERMI LIQUID DESCRIPTION FOR THERMOELECTRIC TRANSPORT OF QD

In this section, we discuss thermoelectric transport through multilevel quantum dots in the linear-response regime, the low-energy behaviors of which can be deduced from the asymptotic form of the spectral function $A_\sigma(\omega)$ given in Appendix B.

The linear conductance g , thermopower \mathcal{S}_{QD} and thermal conductance κ_{QD} of a quantum dot can be expressed in the form [22, 79–82]:

$$g \equiv \frac{dJ}{dV} \Big|_{eV=0} = \frac{e^2}{h} \sum_{\sigma} \mathcal{L}_{0,\sigma}^{\text{QD}}, \quad (4.1)$$

$$\mathcal{S}_{\text{QD}} = \frac{-1}{|e|T} \frac{\sum_{\sigma} \mathcal{L}_{1,\sigma}^{\text{QD}}}{\sum_{\sigma} \mathcal{L}_{0,\sigma}^{\text{QD}}}, \quad (4.2)$$

$$\kappa_{\text{QD}} = \frac{1}{hT} \left[\sum_{\sigma} \mathcal{L}_{2,\sigma}^{\text{QD}} - \frac{\left(\sum_{\sigma} \mathcal{L}_{1,\sigma}^{\text{QD}} \right)^2}{\sum_{\sigma} \mathcal{L}_{0,\sigma}^{\text{QD}}} \right]. \quad (4.3)$$

Here, $\mathcal{L}_{n,\sigma}^{\text{QD}}$ for $n = 0, 1$, and 2 is defined at $eV = 0$ with respect to the thermal equilibrium, as

$$\mathcal{L}_{n,\sigma}^{\text{QD}} = \int_{-\infty}^{\infty} d\omega \omega^n \mathcal{T}_\sigma(\omega) \left(-\frac{\partial f(\omega)}{\partial \omega} \right), \quad (4.4)$$

with $\mathcal{T}_\sigma(\omega)$, the transmission probability defined in Eq. (3.4). Note that thermal conductance κ_{QD} is the linear-response coefficient of the heat current $J_Q = \kappa_{\text{QD}} \delta T$, flowing from the high-temperature side toward the low-temperature side, with δT the temperature difference between the two sides.

The thermoelectric coefficients $\mathcal{L}_{n,\sigma}^{\text{QD}}$ can be calculated, by substituting the low-energy asymptotic form of $A_\sigma(\omega)$, given in Eq. (B3) into $\mathcal{T}_\sigma(\omega)$. At low temperatures, the component $\mathcal{L}_{0,\sigma}^{\text{QD}}$ for $n = 0$, which determines g , is given by

$$\mathcal{L}_{0,\sigma}^{\text{QD}} = \sin^2 \delta_\sigma - c_{T,\sigma} (\pi T)^2 + O(T^4). \quad (4.5)$$

Here, $c_{T,\sigma}$ is the coefficient that we have already described in Eq. (3.7). The next component, $\mathcal{L}_{1,\sigma}^{\text{QD}}$ for $n = 1$, takes the form

$$\mathcal{L}_{1,\sigma}^{\text{QD}} = \frac{\pi\Delta}{3} \rho'_{d\sigma} (\pi T)^2 + O(T^4). \quad (4.6)$$

Here, $\rho'_{d\sigma}$ is the derivative of the density of states with respect to the frequency ω , which can also be written in terms of the phase shift δ_σ and diagonal linear susceptibility $\chi_{\sigma\sigma}$, as shown in Eq. (A6). Thus, the leading-order term of thermopower for quantum dots is given by

$$\mathcal{S}_{\text{QD}} = -\frac{\pi^2}{3} \frac{\sum_{\sigma} \rho'_{d\sigma}}{\sum_{\sigma} \rho_{d\sigma}} \frac{T}{|e|} + O(T^3). \quad (4.7)$$

The thermal conductance κ_{QD} depends on the other component $\mathcal{L}_{2,\sigma}^{\text{QD}}$ for $n = 2$, the low-energy asymptotic form of which is given by

$$\begin{aligned} \mathcal{L}_{2,\sigma}^{\text{QD}} &= \frac{(\pi T)^2}{3} \left[\sin^2 \delta_\sigma + a_{2,\sigma}^{\text{QD}} (\pi T)^2 + O(T^4) \right], \\ a_{2,\sigma}^{\text{QD}} &\equiv \frac{7\pi^2}{5} \left[\cos 2\delta_\sigma \left(\chi_{\sigma\sigma}^2 + \frac{6}{7} \sum_{\sigma'(\neq\sigma)} \chi_{\sigma\sigma'}^2 \right) \right. \\ &\quad \left. - \frac{\sin 2\delta_\sigma}{2\pi} \left(\chi_{\sigma\sigma\sigma}^{[3]} + \frac{5}{21} \sum_{\sigma'(\neq\sigma)} \chi_{\sigma\sigma'\sigma'}^{[3]} \right) \right]. \end{aligned} \quad (4.8)$$

Therefore, the thermal conductance can be calculated up to terms of order T^3 , by substituting these asymptotic forms into Eq. (4.3):

$$\kappa_{\text{QD}} = \frac{\pi^2 T}{3h} \sum_{\sigma=1}^N \left[\sin^2 \delta_\sigma - c_{\kappa,\sigma}^{\text{QD}} (\pi T)^2 + \dots \right], \quad (4.9)$$

$$c_{\kappa,\sigma}^{\text{QD}} = -a_{2,\sigma}^{\text{QD}} + \frac{\pi^2}{3} \frac{\left(\frac{1}{N} \sum_{\sigma''} \chi_{\sigma''\sigma''} \sin 2\delta_{\sigma''} \right)^2}{(\overline{\sin^2 \delta})_{\text{AM}}}. \quad (4.10)$$

Here, the arithmetic mean (AM) of the phase shifts is defined by

$$(\overline{\sin^2 \delta})_{\text{AM}} \equiv \frac{1}{N} \sum_{\sigma} \sin^2 \delta_\sigma. \quad (4.11)$$

Furthermore, the Lorenz number $L_{\text{QD}} \equiv \kappa_{\text{QD}}/(gT)$ can be calculated up to terms of order T^2 :

$$L_{\text{QD}} = \frac{\pi^2}{3e^2} \left[1 - \frac{c_L^{\text{QD}}}{(\overline{\sin^2 \delta})_{\text{AM}}} (\pi T)^2 + O(T^4) \right], \quad (4.12)$$

$$c_L^{\text{QD}} = \frac{1}{N} \sum_{\sigma} (c_{\kappa,\sigma}^{\text{QD}} - c_{T,\sigma}). \quad (4.13)$$

The Wiedemann-Franz law holds between the leading-order terms of the linear conductance g and the thermal conductance κ_{QD} , such that the Lorenz number approaches the universal value $L_{\text{QD}} \xrightarrow{T \rightarrow 0} \pi^2/(3e^2)$ in the low-temperature limit. The Lorenz number deviates from this universal value as temperature increases, exhibiting the T^2 dependence.

V. THREE-BODY CORRELATIONS IN THE $\text{SU}(N)$ SYMMETRIC FERMION LIQUID

This Hamiltonian \mathcal{H} , defined in Sec. II, has an $\text{SU}(N)$ symmetry in the case at which the impurity states become degenerate $\epsilon_{d\sigma} \equiv \epsilon_d$ for all σ and the Coulomb interaction is isotropic $U_{\sigma\sigma'} \equiv U$ for all σ and σ' .

In the atomic limit $v_j \rightarrow 0$ of the $\text{SU}(N)$ symmetric case, the total number of impurity electrons N_d takes an integer value M and exhibits the Coulomb-stair case behavior as a function of ϵ_d . It consists of a series of plateaus of the width U and the height $N_d = M$ for $M = 1, 2, \dots, N-1$, emerging at $-MU < \epsilon_d < -(M-1)U$ around the midpoint $\epsilon_{d,M}^{\text{mid}} \equiv -(M - \frac{1}{2})U$. We will use the following notation for the shifted impurity level ξ_d , which includes the Hartree-Fock energy shift defined with respect to the half filling in such a way that

$$\xi_d \equiv \epsilon_d + \frac{N-1}{2} U. \quad (5.1)$$

The system has an electron-hole symmetry at $\xi_d = 0$. When the tunneling couplings are switched on, the staircase structure emerges for strong interactions $U \gg \Delta$.

In the $\text{SU}(N)$ symmetric case, the linear susceptibilities have two linearly independent components, i.e., the diagonal one $\chi_{\sigma\sigma}$ and the off-diagonal one $\chi_{\sigma\sigma'}$ for $\sigma \neq \sigma'$. These two components determine the essential properties of quasiparticles:

$$T^* \equiv \frac{1}{4\chi_{\sigma\sigma}}, \quad R \equiv 1 - \frac{\chi_{\sigma\sigma'}}{\chi_{\sigma\sigma}}. \quad (5.2)$$

Here, T^* is a characteristic energy scale of the $\text{SU}(N)$ Fermi liquid, by which the T -linear specific heat of impurity electrons can be expressed in the form $\mathcal{C}_{\text{imp}} = \frac{N\pi^2}{12} T/T^*$ [6, 8, 9]. The Wilson ratio R corresponds to a dimensionless residual interaction between quasiparticles [83]; we will also use the rescaled ratio,

$$\tilde{K} \equiv (N-1)(R-1), \quad (5.3)$$

which is bounded in the range $0 \leq \tilde{K} \leq 1$.

A. Charge and spin susceptibilities

The charge susceptibility is given by a linear combination of the two-body correlations,

$$\bar{\chi}_C \equiv -\frac{1}{N} \frac{\partial^2 \Omega}{\partial \epsilon_d^2} = \frac{1}{N} \sum_{\sigma_1 \sigma_2} \chi_{\sigma_1 \sigma_2} \quad (5.4)$$

$$\xrightarrow{\text{SU}(N)} \chi_{\sigma\sigma} + (N-1)\chi_{\sigma\sigma'} = \frac{1 - \tilde{K}}{4T^*}. \quad (5.5)$$

Here, $\Omega \equiv -T \log [\text{Tr} e^{-\mathcal{H}/T}]$ is the free energy.

Next, we consider the spin susceptibility for the $\text{SU}(N)$ symmetric case, using the notation in which the internal degrees of freedom are separated into two parts $\sigma = (m, s)$, where $m = 1, 2, \dots, N/2$ and $s = \uparrow, \downarrow$, assuming N to be even (extension to odd N is straightforward). The Zeeman splitting is induced by an external field b , which couples to the impurity spin s :

$$\epsilon_{d,m,\uparrow} = \epsilon_d - b, \quad \epsilon_{d,m,\downarrow} = \epsilon_d + b. \quad (5.6)$$

The magnetization \mathcal{M} of the impurity spin is given by

$$\mathcal{M} \equiv -\frac{1}{N} \frac{\partial \Omega}{\partial b} = \frac{1}{N} \sum_{m=1}^{\frac{N}{2}} \langle n_{d,m\uparrow} - n_{d,m\downarrow} \rangle. \quad (5.7)$$

Note that Ω is an even function of b . The spin susceptibility $\bar{\chi}_S \equiv -(1/N) \frac{\partial^2 \Omega}{\partial b^2} \Big|_{b=0}$ can be expressed in the following form,

$$\bar{\chi}_S = \frac{1}{N} \sum_{m=1}^{\frac{N}{2}} \sum_{m'=1}^{\frac{N}{2}} \left[\chi_{m\uparrow, m'\uparrow} + \chi_{m\downarrow, m'\downarrow} - \chi_{m\uparrow, m'\downarrow} - \chi_{m\downarrow, m'\uparrow} \right] \quad (5.8)$$

$$\xrightarrow{\text{SU}(N)} \chi_{\sigma\sigma} - \chi_{\sigma\sigma'} = \frac{1}{4T^*} \left(1 + \frac{\tilde{K}}{N-1} \right), \quad (5.9)$$

where $\sigma \neq \sigma'$.

B. Three-body correlation functions

Among N^3 components of the three-body correlation $\chi_{\sigma_1\sigma_2\sigma_3}^{[3]}$, only three components become linearly independent in the $\text{SU}(N)$ symmetric case. They can be expressed in terms of the derivatives of the linear susceptibilities, using Eqs. (C1), (C2), and (C5) given in Appendix C:

$$\chi_{\sigma\sigma\sigma}^{[3]} = \frac{1}{N} \frac{\partial \chi_{\sigma\sigma}}{\partial \epsilon_d} - \frac{N-1}{N} \chi_B^{[3]}, \quad (5.10)$$

$$\tilde{\chi}_{\sigma\sigma'\sigma'}^{[3]} = \frac{N-1}{N} \frac{\partial \chi_{\sigma\sigma}}{\partial \epsilon_d} + \frac{N-1}{N} \chi_B^{[3]}, \quad (5.11)$$

$$\tilde{\chi}_{\sigma\sigma'\sigma''}^{[3]} = -\frac{N-1}{N} \frac{\partial \chi_{\sigma\sigma}}{\partial \epsilon_d} + \frac{N-1}{2} \frac{\partial \chi_{\sigma\sigma'}}{\partial \epsilon_d} - \frac{N-1}{N} \chi_B^{[3]}, \quad (5.12)$$

for $\sigma \neq \sigma' \neq \sigma'' \neq \sigma$. Here,

$$\begin{aligned} \chi_B^{[3]} &\equiv \frac{\partial}{\partial b} \left(\frac{\chi_{m\uparrow, m\uparrow} - \chi_{m\downarrow, m\downarrow}}{2} \right) \Big|_{b=0} \\ &= -\chi_{\sigma\sigma}^{[3]} + \chi_{\sigma\sigma'}^{[3]}, \end{aligned} \quad (5.13)$$

and the scale factors $(N-1)$ and $(N-1)(N-2)/2$ have been introduced for the off-diagonal three-body components in such a way that

$$\tilde{\chi}_{\sigma\sigma'\sigma'}^{[3]} \equiv (N-1) \chi_{\sigma\sigma'\sigma'}^{[3]}, \quad (5.14)$$

$$\tilde{\chi}_{\sigma\sigma'\sigma''}^{[3]} \equiv \frac{(N-1)(N-2)}{2} \chi_{\sigma\sigma'\sigma''}^{[3]}. \quad (5.15)$$

We will also use the dimensionless three-body correlations, defined by

$$\Theta_{\text{I}} \equiv \frac{\sin 2\delta}{2\pi} \frac{\chi_{\sigma\sigma\sigma}^{[3]}}{\chi_{\sigma\sigma}^2}, \quad \tilde{\Theta}_{\text{II}} \equiv \frac{\sin 2\delta}{2\pi} \frac{\tilde{\chi}_{\sigma\sigma'\sigma'}^{[3]}}{\chi_{\sigma\sigma}^2}, \quad (5.16)$$

$$\tilde{\Theta}_{\text{III}} \equiv \frac{\sin 2\delta}{2\pi} \frac{\tilde{\chi}_{\sigma\sigma'\sigma''}^{[3]}}{\chi_{\sigma\sigma}^2}. \quad (5.17)$$

TABLE I. Low-energy expansion of transport coefficients through $\text{SU}(N)$ quantum dots (QD) and magnetic alloys (MA), described in Eqs. (5.19)–(5.22) and Eqs. (9.2)–(9.4). Here, $T^* \equiv 1/(4\chi_{\sigma\sigma})$ is a characteristic FL energy scale.

$\frac{dJ}{dV} = \frac{Ne^2}{h} \left[\sin^2 \delta - C_T \left(\frac{\pi T}{T^*} \right)^2 - C_V \left(\frac{eV}{T^*} \right)^2 + \dots \right]$
$S_{\text{noise}}^{\text{QD}} = \frac{2Ne^2 eV }{h} \left[\sin^2 \delta (1 - \sin^2 \delta) + C_S \left(\frac{eV}{T^*} \right)^2 + \dots \right]$
$\kappa_{\text{QD}} = \frac{N\pi^2 T}{3h} \left[\sin^2 \delta - C_{\kappa}^{\text{QD}} \left(\frac{\pi T}{T^*} \right)^2 + \dots \right]$
$L_{\text{QD}} \equiv \frac{\kappa_{\text{QD}}}{gT} = \frac{\pi^2}{3e^2} \left[1 - \frac{C_L^{\text{QD}}}{\sin^2 \delta} \left(\frac{\pi T}{T^*} \right)^2 + \dots \right]$
$\varrho_{\text{MA}} \equiv \frac{1}{\sigma_{\text{MA}}} = \frac{1}{\sigma_{\text{MA}}^{\text{unit}}} \left[\sin^2 \delta - C_{\varrho}^{\text{MA}} \left(\frac{\pi T}{T^*} \right)^2 + \dots \right]$
$\frac{1}{\kappa_{\text{MA}}} = \frac{3e^2}{\pi^2 \sigma_{\text{MA}}^{\text{unit}} T} \left[\sin^2 \delta - C_{\kappa}^{\text{MA}} \left(\frac{\pi T}{T^*} \right)^2 + \dots \right]$
$L_{\text{MA}} \equiv \frac{\kappa_{\text{MA}}}{\sigma_{\text{MA}} T} = \frac{\pi^2}{3e^2} \left[1 - \frac{C_L^{\text{MA}}}{\sin^2 \delta} \left(\frac{\pi T}{T^*} \right)^2 + \dots \right]$

In this work, we calculate the right-hand side of Eqs. (5.10)–(5.12) with the NRG to obtain the three-body correlations for the $\text{SU}(N)$ case. Note that, for noninteracting electrons at $U=0$, only the diagonal components of the three-body correlation Θ_{I}^0 and the susceptibility $\chi_{\sigma\sigma}^0$ remain finite due to the Pauli exclusion principle,

$$\Theta_{\text{I}}^0 = \frac{-2\epsilon_d^2}{\epsilon_d^2 + \Delta^2}, \quad \chi_{\sigma\sigma}^0 = \frac{1}{\pi} \frac{\Delta}{\epsilon_d^2 + \Delta^2}, \quad (5.18)$$

and $T^* \xrightarrow{U \rightarrow 0} \pi \Delta [1 + (\epsilon_d/\Delta)^2]/4$.

C. Transport formulas for quantum dots in $\text{SU}(N)$ Fermi liquid regime

We next consider the low-energy expansion of transport coefficients dJ/dV , $S_{\text{noise}}^{\text{QD}}$, κ_{QD} , and the Lorenz number L_{QD} . Specifically, for the junctions having tunneling and bias symmetries $\Gamma_L = \Gamma_R$ and $\mu_L = -\mu_R = eV/2$, these transport coefficients take the following form in the $\text{SU}(N)$ symmetric case,

$$\frac{dJ}{dV} = \frac{Ne^2}{h} \left[\sin^2 \delta - C_T \left(\frac{\pi T}{T^*} \right)^2 - C_V \left(\frac{eV}{T^*} \right)^2 + \dots \right], \quad (5.19)$$

$$S_{\text{noise}}^{\text{QD}} = \frac{2Ne^2|eV|}{h} \left[\frac{\sin^2 2\delta}{4} + C_S \left(\frac{eV}{T^*} \right)^2 + \dots \right], \quad (5.20)$$

$$\kappa_{\text{QD}} = \frac{N\pi^2 T}{3h} \left[\sin^2 \delta - C_{\kappa}^{\text{QD}} \left(\frac{\pi T}{T^*} \right)^2 + \dots \right], \quad (5.21)$$

$$L_{\text{QD}} = \frac{\pi^2}{3e^2} \left[1 - \frac{C_L^{\text{QD}}}{\sin^2 \delta} \left(\frac{\pi T}{T^*} \right)^2 + \dots \right]. \quad (5.22)$$

The formulas for the coefficients C_T , C_V , C_S , C_{κ}^{QD} , and C_L^{QD} of the next-leading order terms are summarized in

TABLE II. Coefficients C 's for the next-leading order terms of $SU(N)$ quantum dots and magnetic alloys (MA), summarized in Table I. In these formulas, W 's represent the contributions determined by the phase shift δ and the rescaled Wilson ratio $\tilde{K} = (N-1)(R-1)$. Three-body correlations enter through $\Theta_I \equiv \frac{\sin 2\delta}{2\pi} \frac{\chi_{\sigma\sigma\sigma}^{[3]}}{\chi_{\sigma\sigma}^2}$ and $\tilde{\Theta}_{II} \equiv \frac{\sin 2\delta}{2\pi} \frac{\tilde{\chi}_{\sigma\sigma'\sigma'}^{[3]}}{\chi_{\sigma\sigma}^2}$.

$C_T = \frac{\pi^2}{48} [W_T + \Theta_I + \tilde{\Theta}_{II}]$	$W_T \equiv - \left[1 + \frac{2\tilde{K}^2}{N-1} \right] \cos 2\delta$
$C_V = \frac{\pi^2}{64} [W_V + \Theta_I + 3\tilde{\Theta}_{II}]$	$W_V \equiv - \left[1 + \frac{5\tilde{K}^2}{N-1} \right] \cos 2\delta$
$C_S = \frac{\pi^2}{192} [W_S - \cos 2\delta \{ \Theta_I + 3\tilde{\Theta}_{II} \}]$	$W_S \equiv \cos 4\delta + \left[4 + 5 \cos 4\delta + \frac{3}{2}(1 - \cos 4\delta)(N-2) \right] \frac{\tilde{K}^2}{N-1}$
$C_\kappa^{\text{QD}} = \frac{7\pi^2}{80} [W_\kappa^{\text{QD}} + \Theta_I + \frac{5}{21}\tilde{\Theta}_{II}]$	$W_\kappa^{\text{QD}} \equiv \frac{10-11\cos 2\delta}{21} - \frac{6}{7} \frac{\tilde{K}^2}{N-1} \cos 2\delta$
$C_L^{\text{QD}} = \frac{\pi^2}{240} [W_L^{\text{QD}} + 16\Theta_I] = C_\kappa^{\text{QD}} - C_T$	$W_L^{\text{QD}} \equiv 10 - 6 \cos 2\delta - \frac{8\tilde{K}^2}{N-1} \cos 2\delta$
$C_e^{\text{MA}} = \frac{\pi^2}{48} [W_e^{\text{MA}} + \Theta_I + \tilde{\Theta}_{II}]$	$W_e^{\text{MA}} \equiv 2 + \cos 2\delta - \frac{2\tilde{K}^2}{N-1} \cos 2\delta = 4 \cos^2 \delta + W_T$
$C_\kappa^{\text{MA}} = \frac{7\pi^2}{80} [W_\kappa^{\text{MA}} + \Theta_I + \frac{5}{21}\tilde{\Theta}_{II}]$	$W_\kappa^{\text{MA}} \equiv \frac{32+11\cos 2\delta}{21} - \frac{6}{7} \frac{\tilde{K}^2}{N-1} \cos 2\delta = \frac{44}{21} \cos^2 \delta + W_\kappa^{\text{QD}}$
$C_L^{\text{MA}} = \frac{\pi^2}{240} [W_L^{\text{MA}} - 16\Theta_I] = C_e^{\text{MA}} - C_\kappa^{\text{MA}}$	$W_L^{\text{MA}} \equiv -22 - 6 \cos 2\delta + \frac{8\tilde{K}^2}{N-1} \cos 2\delta = -24 \cos^2 \delta - W_L^{\text{QD}}$

Tables I and II. Each of these C 's can be decomposed into two parts, denoted as W 's and Θ 's. The W part, defined in the right column of Table II, represents the two-body contributions determined by \tilde{K} and δ . The Θ part represents the three-body contributions which can be described in terms of the dimensionless parameters defined in Eq. (5.16).

These transport formulas in the $SU(N)$ Fermi liquid regime clarify the fact that the next-leading order terms for the symmetric tunnel junctions are completely determined by *five* parameters: δ , T^* , \tilde{K} , Θ_I , and $\tilde{\Theta}_{II}$. The three-body correlations can be experimentally deduced through the measurements of the coefficients C 's. The other three-body component, $\tilde{\Theta}_{III}$, defined with respect to three different levels, couples to the tunnel and bias asymmetries, i.e., $\Gamma_L \neq \Gamma_R$ and $\mu_L \neq -\mu_R$, and contributes to the nonlinear current [28, 29]. The behavior of C 's depend significantly on the electron filling N_d of the impurity levels. For instance, in the noninteracting case at $U = 0$, these coefficients vary with the level position ϵ_d as shown in Fig. 1.

In the rest of this paper, we will demonstrate the be-

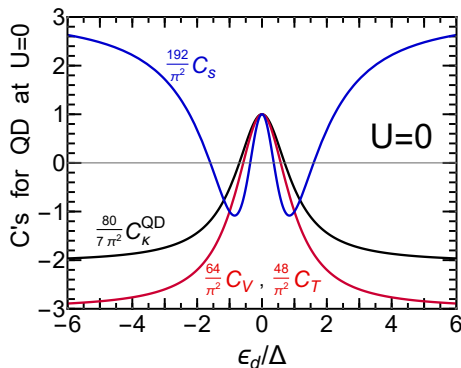


FIG. 1. Coefficients C_V , C_T , C_S , and C_κ^{QD} for noninteracting $U = 0$ quantum dots plotted vs ϵ_d .

havior of the next-leading order terms of the transport coefficients for $N = 4$ and 6 . To this end, we calculate the correlation functions δ , $\chi_{\sigma_1\sigma_2}$, and $\chi_{\sigma_1\sigma_2\sigma_3}^{[3]}$ using the NRG approach [26, 84], with parameter settings described in Appendix D. Specifically, Eqs. (5.10)–(5.13) are used for obtaining the three-body correlations. We have reported part of the results for coefficient C_V in a previous paper, studying the role of bias and tunneling asymmetries on the nonlinear terms of dJ/dV at $T = 0$ [29]. In this paper, we provide a comprehensive view of the three-body Fermi liquid effect through a systematic analysis of the next-leading order terms C_S , C_T , and C_κ^{QD} for quantum dots, and through the related coefficients for magnetic alloys, C_e^{MA} , and C_κ^{MA} . In order to quickly grasp the underlying physics derived from quasiparticle properties in the $SU(4)$ and $SU(6)$ cases, we provide a brief review of the key characteristics of the two-body correlation functions in Appendix E, extending the interaction range up to $U/(\pi\Delta) = 6.0$. Additionally, we also include some new results for the renormalized impurity level $\tilde{\epsilon}_{d\sigma}$ there.

VI. THREE-BODY CORRELATIONS IN THE $SU(4)$ & $SU(6)$ ANDERSON IMPURITY

In this section, we discuss the behavior of charge and spin susceptibilities defined in Eqs. (5.5) and (5.9). In particular, we focus on the derivatives $\partial\bar{\chi}_C/\partial\epsilon_d$ and $\partial\bar{\chi}_S/\partial\epsilon_d$, which can also be expressed in terms of the three-body correlation functions:

$$\frac{\partial\bar{\chi}_C}{\partial\epsilon_d} = \chi_{\sigma\sigma\sigma}^{[3]} + 3\tilde{\chi}_{\sigma\sigma'\sigma'}^{[3]} + 2\tilde{\chi}_{\sigma\sigma'\sigma''}^{[3]}, \quad (6.1)$$

$$\frac{\partial\bar{\chi}_S}{\partial\epsilon_d} = \chi_{\sigma\sigma\sigma}^{[3]} + \frac{N-3}{N-1}\tilde{\chi}_{\sigma\sigma'\sigma'}^{[3]} - \frac{2}{N-1}\tilde{\chi}_{\sigma\sigma'\sigma''}^{[3]}. \quad (6.2)$$

The NRG results reveal the fact that these derivatives in the left-hand side are suppressed in the strong-coupling

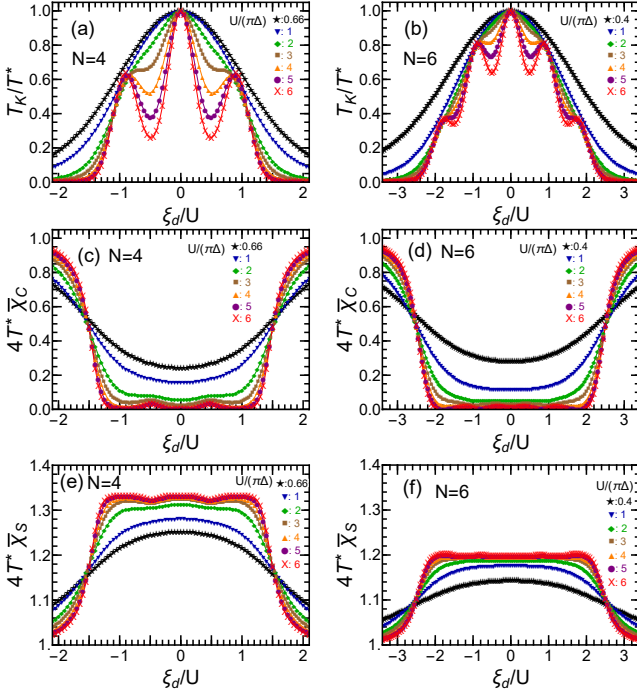


FIG. 2. Inverse energy scale $1/T^*$, charge susceptibility $\bar{\chi}_C$ and spin $\bar{\chi}_S$ susceptibilities are plotted vs ξ_d ($= \epsilon_d + U/2$) for $N = 4$ and 6 . Here, $4T^*$ ($= 1/\chi_{\sigma\sigma}$), and $T_K \equiv T^*|_{\xi_d=0}$. Interaction strengths are chosen such that, for $N = 4$, $U/(\pi\Delta) = 2/3(\star)$, $1(\blacktriangledown)$, $2(\blacklozenge)$, $3(\blacksquare)$, $4(\blacktriangle)$, $5(\bullet)$, and $6(\times)$, at which $T_K/(\pi\Delta) = 0.20, 0.18, 0.13, 0.092, 0.063, 0.041$, and 0.026 , respectively. For $N = 6$, $U/(\pi\Delta) = 2/5(\star)$, $1(\blacktriangledown)$, $2(\blacklozenge)$, $3(\blacksquare)$, $4(\blacktriangle)$, $5(\bullet)$, and $6(\times)$, at which $T_K/(\pi\Delta) = 0.22, 0.19, 0.15, 0.13, 0.10, 0.085$, and 0.068 , respectively.

region $|\xi_d| \lesssim (N-1)U/2$ for large U . This implies that the linear combinations of the three-body correlations in left-hand side of Eqs. (6.1) and (6.2) approach zero, reducing the number of independent components of the three-body correlation functions $\chi_{\sigma_1\sigma_2\sigma_3}^{[3]}$, as demonstrated below.

A. Charge and spin susceptibilities: $\bar{\chi}_C$ & $\bar{\chi}_S$

One of the most fundamental quantities that play a central role in the low-energy physics of quantum impurities is the characteristic energy scale $T^* \equiv 1/(4\chi_{\sigma\sigma})$, defined in Eq. (5.2) as an inverse of the diagonal susceptibility $N\chi_{\sigma\sigma} = \bar{\chi}_C + (N-1)\bar{\chi}_S$. We will use, in the following discussions, the Kondo temperature $T_K \equiv T^*|_{\xi_d=0}$, defined as the value of T^* at the electron-hole symmetric point $\xi_d = 0$.

The NRG results for $1/T^*$ in the SU(4) and SU(6) cases are plotted vs ξ_d in Figs. 2(a) and 2(b), respectively, by multiplying them by T_K . We see that $1/T^*$ has $N-1$ local maxima for strong interactions, at integer-filling points, i.e., $\xi_d \simeq 0, \pm U, \dots, \pm(N-2)U/2$, reflecting the oscillatory behavior of the wave function renormalization

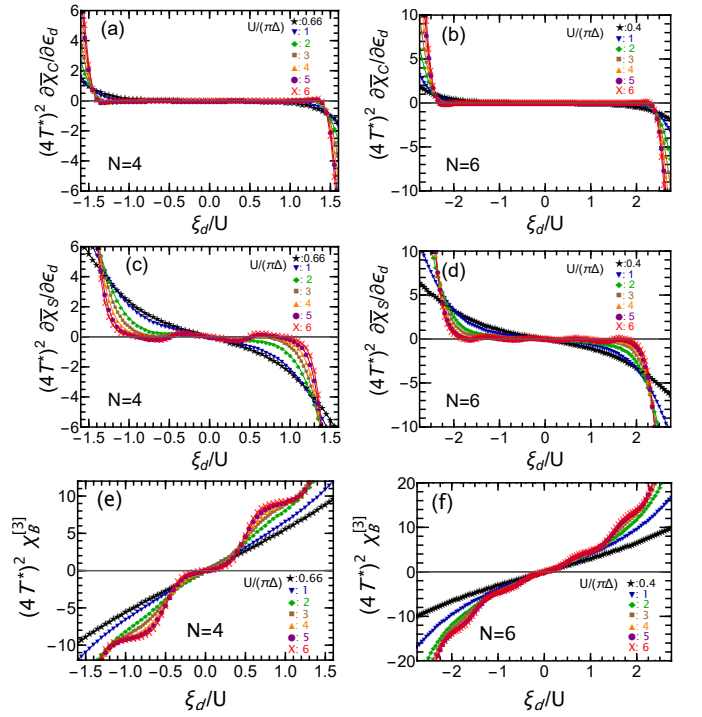


FIG. 3. $(4T^*)^2 \partial \bar{\chi}_C / \partial \epsilon_d$, $(4T^*)^2 \partial \bar{\chi}_S / \partial \epsilon_d$, and $(4T^*)^2 \chi_B^{[3]}$ are plotted vs ξ_d for $N = 4$ and 6 . Interaction strengths are chosen such that, for $N = 4$, $U/(\pi\Delta) = 2/3(\star)$, $1(\blacktriangledown)$, $2(\blacklozenge)$, $3(\blacksquare)$, $4(\blacktriangle)$, $5(\bullet)$, $6(\times)$. For $N = 6$, $U/(\pi\Delta) = 2/5(\star)$, $1(\blacktriangledown)$, $2(\blacklozenge)$, $3(\blacksquare)$, $4(\blacktriangle)$, $5(\bullet)$, $6(\times)$.

factor z ($= \rho_{d\sigma}/\chi_{\sigma\sigma}$) described in Appendix E. At $|\xi_d| \gg (N-1)U/2$, the energy scale T^* approaches the non-interacting value, $T_K/T^* \xrightarrow{|\xi_d| \gg (N-1)U/2} \Delta^2/\xi_d^2$, as the electron filling of the impurity levels approaches $N_d \simeq 0$ or N .

The charge susceptibilities for $N = 4$ and 6 are plotted in Figs. 2(c) and 2(d), using T^* as a normalization factor, i.e., $4T^*\bar{\chi}_C = 1 - \tilde{K}$ from Eq. (5.5). Therefore, the normalized value $4T^*\bar{\chi}_C$ is determined by the rescaled Wilson ratio \tilde{K} , described in Appendix E. As U increases, $4T^*\bar{\chi}_C$ decreases in a wide region of the impurity level $|\xi_d| \lesssim (N-1)U/2$, where the impurity levels are partially filled $1 \lesssim N_d \lesssim N-1$. In this filling range, the charge susceptibility is significantly suppressed by the Coulomb repulsion, and it vanishes $4T^*\bar{\chi}_C \xrightarrow{U \gg \pi\Delta} 0$ in the strong interaction limit. Outside this region, i.e., at $|\xi_d| \gg (N-1)U/2$, the charge susceptibility approaches the noninteracting value $4T^*\bar{\chi}_C \xrightarrow{|\xi_d| \rightarrow \infty} 1$ as the filling of the impurity levels approaches $N_d \simeq 0$ or N .

Figures 2(e) and 2(f) show the spin susceptibilities for $N = 4$ and 6 , which are normalized with the same scaling factor, i.e., $4T^*\bar{\chi}_S = 1 + \tilde{K}/(N-1)$ [see Eq. (5.9)]. As the interaction U increases, $4T^*\bar{\chi}_S$ increases from the non-interacting value 1. In the strong interaction limit, it approaches the value $4T^*\bar{\chi}_S \rightarrow N/(N-1)$, i.e., $4/3$ for $N = 4$ and $6/5$ for $N = 6$, and exhibits a wide plateau

structure in the strong-coupling region $|\xi_d| \lesssim (N-1)U/2$. At $|\xi_d| \gg (N-1)U/2$, where the occupation number approaches $N_d \simeq 0$ or N , the spin susceptibility also approaches the noninteracting value $4T^*\bar{\chi}_S \xrightarrow{|\xi_d| \rightarrow \infty} 1$.

B. Derivative of $\bar{\chi}_C$ and $\bar{\chi}_S$ with respect to ϵ_d

The three-body correlation functions can be obtained from the derivatives of $\chi_{\sigma_1\sigma_2}$ with respect to ϵ_d and b , using Eqs. (5.10)–(5.12). In particular, $\partial\chi_{\sigma_1\sigma_2}/\partial\epsilon_d$ can be rewritten in terms of the derivatives of the charge and spin susceptibilities, as

$$\frac{\partial\chi_{\sigma\sigma}}{\partial\epsilon_d} = \frac{1}{N} \frac{\partial\bar{\chi}_C}{\partial\epsilon_d} + \frac{N-1}{N} \frac{\partial\bar{\chi}_S}{\partial\epsilon_d}, \quad (6.3)$$

$$(N-1) \frac{\partial\chi_{\sigma\sigma'}}{\partial\epsilon_d} = \frac{N-1}{N} \frac{\partial\bar{\chi}_C}{\partial\epsilon_d} - \frac{N-1}{N} \frac{\partial\bar{\chi}_S}{\partial\epsilon_d}, \quad (6.4)$$

for $\sigma \neq \sigma'$. Figures 3(a) and 3(b) show the NRG results for $\partial\bar{\chi}_C/\partial\epsilon_d$ for $N=4$ and 6 , respectively. Similarly, the derivatives of the spin susceptibility $\partial\bar{\chi}_S/\partial\epsilon_d$ for $N=4$ and 6 are plotted in Figs. 3(c) and 3(d). Note that in these figures, the derivatives have been multiplied by a factor of $(4T^*)^2$ to make them dimensionless. These derivatives are significantly suppressed in the strong-coupling region $|\xi_d| \lesssim (N-1)U/2$ for large U . More specifically, $|\partial\bar{\chi}_C/\partial\epsilon_d| \ll |\partial\bar{\chi}_S/\partial\epsilon_d| \ll 1/(4T^*)^2$: the derivative of spin susceptibility becomes much smaller than $1/(4T^*)^2$ while it is still larger than the derivative of charge susceptibility. Therefore, both $\partial\chi_{\sigma\sigma}/\partial\epsilon_d$ and $\partial\chi_{\sigma\sigma'}/\partial\epsilon_d$ are suppressed in a wide range of electron fillings $1 \lesssim N_d \lesssim N-1$ for large U .

We next consider $\chi_B^{[3]}$, defined in Eq. (5.13) as a derivative of a linear combination of the two different diagonal susceptibilities with respect to the magnetic fields b . Figures 3(e) and 3(f) show $(4T^*)^2\chi_B^{[3]}$ for $N=4$ and 6 , respectively. We see that $(4T^*)^2\chi_B^{[3]}$ exhibits a staircase structure with a flat plateau emerging around the integer filling points $\xi_d = 0, \pm U, \pm 2U, \dots, (N-2)U/2$ for large U . The magnitude $|\chi_B^{[3]}|$ becomes much larger than the derivative of the charge and spin susceptibilities, $|\partial\bar{\chi}_C/\partial\epsilon_d|$ and $|\partial\bar{\chi}_S/\partial\epsilon_d|$. Therefore, $\chi_B^{[3]}$ dominates the terms in the right-hand side of Eqs. (5.10)–(5.12) in the strong-coupling region $|\xi_d| \lesssim (N-1)U/2$, and the three independent components of three-body correlations approach one another in such a way that

$$\chi_{\sigma\sigma\sigma}^{[3]} \simeq -\tilde{\chi}_{\sigma\sigma'\sigma'}^{[3]} \simeq \tilde{\chi}_{\sigma\sigma'\sigma''}^{[3]} \simeq -\frac{N-1}{N} \chi_B^{[3]}. \quad (6.5)$$

This means that the three-body correlations are described by a single parameter $\chi_B^{[3]}$ in a wide filling range $1 \lesssim N_d \lesssim N-1$ for large U .

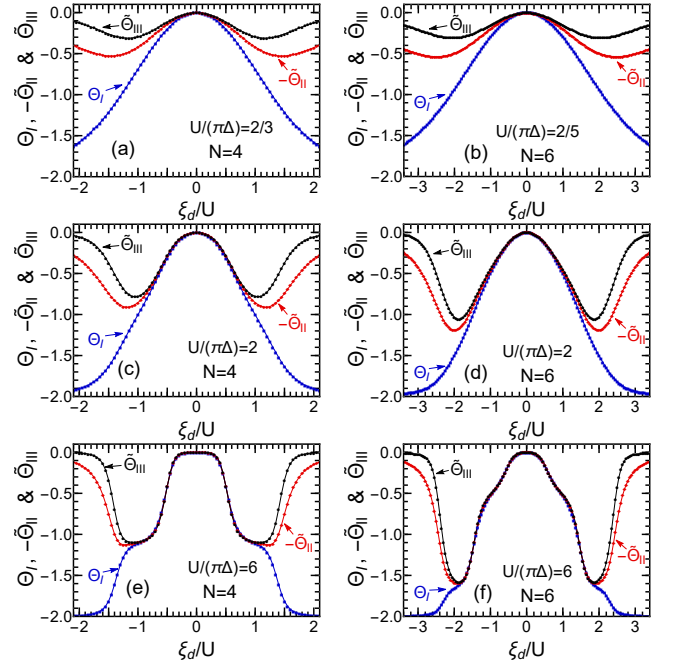


FIG. 4. Dimensionless three-body corrections Θ_I (■), $-\Theta_{II}$ (◆), and Θ_{III} (●) are plotted vs ξ_d , for interaction strengths $U/(\pi\Delta) = 2/3$ (a), $2/5$ (b), 2 (c,d), and 6 (e,f).

C. Three-body correlations for $N=4$ and 6

We have calculated the three-body correlation functions $\chi_{\sigma\sigma\sigma}^{[3]}$, $\tilde{\chi}_{\sigma\sigma'\sigma'}^{[3]}$ and $\tilde{\chi}_{\sigma\sigma'\sigma''}^{[3]}$ for $\sigma \neq \sigma' \neq \sigma'' \neq \sigma$, using Eqs. (5.10)–(5.12). Figure 4 shows the dimensionless three-body correlations Θ_I , $\tilde{\Theta}_{II}$ and $\tilde{\Theta}_{III}$, defined in Eqs. (5.16) and (5.17). The left and right panels describe the NRG results in the SU(4) and SU(6) cases, respectively, and three different interaction strengths (from weak to strong) are chosen for the top, middle, and bottom panels.

All components of the three-body correlation functions vanish, $\Theta_I = \tilde{\Theta}_{II} = \tilde{\Theta}_{III} = 0$, at the electron-hole symmetric point $\xi_d = 0$, and evolve as ξ_d deviates from this point. Among the three independent components, the intra-level component Θ_I has the largest magnitude, and exhibits plateau structures for large U at integer filling points $N_d \simeq 1, 2, \dots, N-1$. The other components, $\tilde{\Theta}_{II}$ and $\tilde{\Theta}_{III}$, involve inter-level correlations and evolve as the Coulomb interaction U increases. In particular, the correlation between the three different levels $\tilde{\Theta}_{III}$ becomes the weakest. In the limit of $|\xi_d| \rightarrow \infty$, the diagonal component Θ_I approaches the noninteracting value while the other two vanish:

$$\Theta_I \xrightarrow{|\xi_d| \rightarrow \infty} -2, \quad \tilde{\Theta}_{II} \xrightarrow{|\xi_d| \rightarrow \infty} 0, \quad \tilde{\Theta}_{III} \xrightarrow{|\xi_d| \rightarrow \infty} 0. \quad (6.6)$$

Figures 4(e) and 4(f) clearly demonstrate the relation

Eq. (6.5), which holds at $|\xi_d| \lesssim (N-1)U/2$ for large U :

$$\Theta_I \simeq -\tilde{\Theta}_{II} \simeq \tilde{\Theta}_{III}. \quad (6.7)$$

It means that all the three-body components are determined by a single parameter $\chi_B^{[3]}$ in the strong-coupling region for large U , as mentioned. The dimensionless three-body correlation functions clearly exhibit the plateau structure around the integer filling points $\xi_d = 0, \pm U, \pm 2U, \dots, \pm(N-2)U/2$, where the $SU(N)$ Kondo effect occurs. These structures reflect the behavior of $\chi_B^{[3]}$, described in Figs. 3(e) and 3(f), and evolve as the interaction strength U increases. We see, in Figs. 4(e) and 4(f), that the plateaus appear much clearer for $N=4$ than $N=6$, for the same interaction strength $U/(\pi\Delta) = 6.0$.

We will examine, in the subsequent sections, how these three-body correlation functions affect the next-leading order terms of the transport coefficients in the low-energy Fermi liquid regime away from half filling.

VII. NONLINEAR CURRENT NOISE OF $SU(4)$ & $SU(6)$ QUANTUM DOTS

In this section, we discuss the nonlinear terms of the steady current J and the current noise $S_{\text{noise}}^{\text{QD}}$, specifically, the order $(eV)^3$ term for symmetric junctions, i.e., $\Gamma_L = \Gamma_R$ and $\mu_L = -\mu_R = eV/2$. To provide a comprehensive view of the low-bias behavior of these terms, we begin with a brief review on the previous results for the coefficient C_V of the nonlinear conductance [29], extending slightly the interaction range up to $U/(\pi\Delta) = 6.0$. We will then discuss the results for C_S , i.e., the order $|eV|^3$ term of nonlinear noise.

A. C_V : order $(eV)^2$ term of dJ/dV

The leading-order term of the conductance, at $T = 0$, is determined by the transmission probability $\sin^2 \delta$, i.e., the first term in the right-hand side of Eq. (5.19). It exhibits the well-known Kondo plateaus, which develop in the strong-coupling region, as shown in Figs. 15(b) and 16(b) in Appendix E.

The next-leading order term C_V of the nonlinear conductance can be decomposed into the two-body part W_V , defined in Table II, and the three-body part Θ_V , as

$$C_V = \frac{\pi^2}{64} (W_V + \Theta_V), \quad \Theta_V \equiv \Theta_I + 3\tilde{\Theta}_{II}. \quad (7.1)$$

These coefficients C_V , W_V and Θ_V are plotted vs ξ_d in Figs. 5(a)–5(f) for $N=4$ and 6.

The two-body part W_V dominates the next-leading order term near the electron-hole symmetric point $\xi_d = 0$, where $\delta = \pi/2$ and the three-body part Θ_V vanishes:

$$W_V \xrightarrow{\xi_d=0} 1 + \frac{5\tilde{K}^2}{N-1}, \quad \Theta_V \xrightarrow{\xi_d=0} 0. \quad (7.2)$$

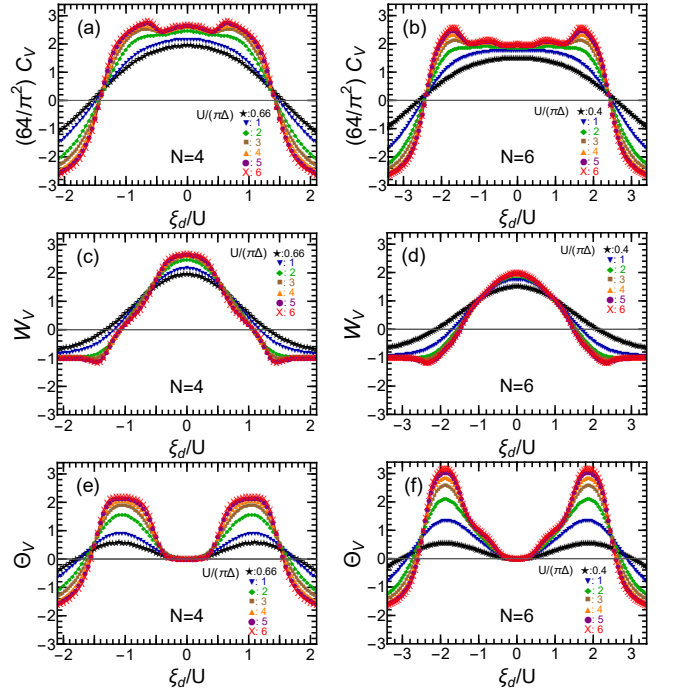


FIG. 5. ξ_d dependence of $C_V = (\pi^2/64)(W_V + \Theta_V)$, two-body part W_V , and three-body part $\Theta_V \equiv \Theta_I + 3\tilde{\Theta}_{II}$. Left panels: $N=4$, for $U/(\pi\Delta) = 2/3$ (\star), 1 (\blacktriangledown), 2 (\blacklozenge), 3 (\blacksquare), 4 (\blacktriangle), 5 (\bullet), 6 (\times). Right panels: $N=6$, for $U/(\pi\Delta) = 2/5$ (\star), 1 (\blacktriangledown), 2 (\blacklozenge), 3 (\blacksquare), 4 (\blacktriangle), 5 (\bullet), 6 (\times).

Therefore, in the strong interaction limit, the peak at $\xi_d = 0$ reaches $(64/\pi^2)C_V \xrightarrow{\xi_d=0 \& U \rightarrow \infty} 8/3$ and 2 for $N=4$ and 6 , respectively. Note that the rescaled Wilson ratio approaches $\tilde{K} \simeq 1$ in a wide region of $|\xi_d| \lesssim (N-1)U/2$ for large U . Outside this region, the two-body and three-body parts of C_V approach to the noninteracting values,

$$W_V \xrightarrow{|\xi_d| \rightarrow \infty} -1, \quad \Theta_V \xrightarrow{|\xi_d| \rightarrow \infty} -2, \quad (7.3)$$

since $\cos 2\delta \xrightarrow{|\xi_d| \rightarrow \infty} 1$, $\tilde{K} \xrightarrow{|\xi_d| \rightarrow \infty} 0$, and the three-body contributions approach the values given in Eq. (6.6).

The $SU(N)$ Kondo effect occurs in the strong-coupling region $|\xi_d| \lesssim (N-1)U/2$ at the integer filling points. The plateau structure evolves as U increases, especially in the three-body part Θ_V , as seen in Figs. 5(e) and 5(f). In the strong-coupling region, it can be expressed in the form $\Theta_V \simeq -2\Theta_I$ due to Eq. (6.7). The two-body part W_V , shown in Figs. 5(c) and 5(d) for $U/(\pi\Delta) \leq 6.0$, does not exhibit a clear plateau other than the one appearing near half filling. For $N=4$, this is because the factor $\cos 2\delta$ for W_V vanishes at $\delta = \pi/4$ and $3\pi/4$, i.e., at the quarter and three-quarters filling points. As a sum of W_V and Θ_V , the coefficient C_V exhibits a wide and rather flat structure in the region of $|\xi_d| \lesssim (N-1)U/2$ for large U , seen in Figs. 5(a) and 5(b). There also emerge some weak local maxima in this flat structure at the integer filling

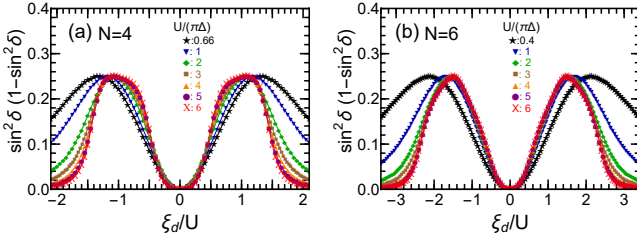


FIG. 6. Linear part, $\sin^2 \delta (1 - \sin^2 \delta)$, of the noise $S_{\text{noise}}^{\text{QD}}$. Interaction strengths are chosen for (a) $N = 4$ to be $U/(\pi\Delta) = 2/3(\star)$, $1(\blacktriangledown)$, $2(\blacklozenge)$, $3(\blacksquare)$, $4(\blacktriangle)$, $5(\bullet)$, $6(\times)$. For (b) $N = 6$, $U/(\pi\Delta) = 2/5(\star)$, $1(\blacktriangledown)$, $2(\blacklozenge)$, $3(\blacksquare)$, $4(\blacktriangle)$, $5(\bullet)$, $6(\times)$.

points $\xi_d = 0, \pm U, \pm 2U, \dots, \pm(N-2)U/2$. In particular, the peak is most pronounced at $\xi_d \simeq \pm(N-2)U/2$, where $N_d \simeq 1$ or $N-1$.

B. Order $|eV|$ and Order $|eV|^3$ terms of $S_{\text{noise}}^{\text{QD}}$

We next consider the current noise $S_{\text{noise}}^{\text{QD}}$, the low-energy asymptotic form of which is given in Eq. (5.20) and Table II. The leading-order term, $\sin^2 \delta (1 - \sin^2 \delta) = (1 - \cos 4\delta)/8$, corresponds to the linear-response noise, the NRG results for which are shown as a function of ξ_d in Figs. 6(a) and 6(b), for $N = 4$ and 6 , respectively. The linear noise is maximized at the points where the phase shift reaches $\delta = \pi/4$ and $3\pi/4$. It occurs at the integer filling points $N_d = 1$ and 3 for $N = 4$, at which the $SU(4)$ Kondo effect makes the peaks wide and flat. In contrast, for $N = 6$, the peak emerges at the half-integer filling points $N_d = 3/2$ and $9/2$. More generally, the peak of the linear noise forms a flat plateau structure for $N \equiv 0 \pmod{4}$, whereas the peak becomes round for $N \equiv 2 \pmod{4}$ due to the fluctuations occurring between two adjacent integer filling states. For large U , the quarter and three-quarters fillings occur near $|\xi_d|/U \simeq N/4$, at which the ground state is highly correlated for multilevel systems of $N \geq 4$. In contrast, these fillings occur at $\xi_d \simeq \pm U/2$ for $SU(2)$ quantum dots, where the electron correlation becomes less important due to the valence fluctuations (see Appendix F).

The coefficient C_S for the order $|eV|^3$ term of current noise $S_{\text{noise}}^{\text{QD}}$ can also be decomposed into the two-body W_S and three-body Θ_S parts, as shown in Table II:

$$C_S = \frac{\pi^2}{192} (W_S + \Theta_S), \quad \Theta_S \equiv -(\Theta_I + 3\tilde{\Theta}_{II}) \cos 2\delta. \quad (7.4)$$

The behavior of three-body part Θ_S can be deduced from the one for dJ/dV , i.e., $\Theta_V = \Theta_I + 3\tilde{\Theta}_{II}$ shown in Figs. 5(e) and 5(f), by multiplying them by a factor of “ $-\cos 2\delta$ ” which induces the modulations. One of the most distinctive features of C_S , compared to the other coefficients C 's listed in Table II, is that it depends upon the higher harmonics $\cos 4\delta$ and $\sin 4\delta$ with

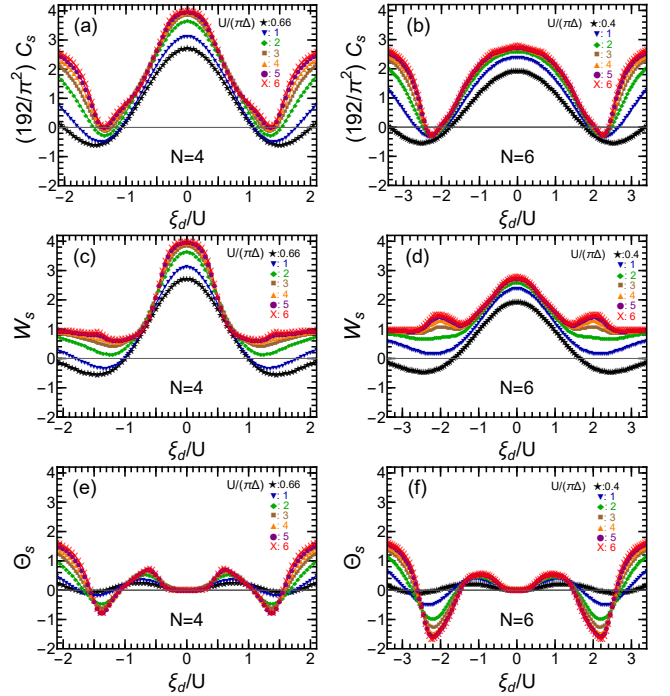


FIG. 7. ξ_d dependence of $C_S = (\pi^2/192)(W_S + \Theta_S)$, two-body part W_S , and three-body part $\Theta_S \equiv -(\Theta_I + 3\tilde{\Theta}_{II}) \cos 2\delta$. Left panels: $N = 4$, for $U/(\pi\Delta) = 2/3(\star)$, $1(\blacktriangledown)$, $2(\blacklozenge)$, $3(\blacksquare)$, $4(\blacktriangle)$, $5(\bullet)$, $6(\times)$. Right panels: $N = 6$, for $U/(\pi\Delta) = 2/5(\star)$, $1(\blacktriangledown)$, $2(\blacklozenge)$, $3(\blacksquare)$, $4(\blacktriangle)$, $5(\bullet)$, $6(\times)$.

respect to the phase shift, which enter through not only through W_S but Θ_S : note that Θ_I and $\tilde{\Theta}_{II}$ defined in Eq. (5.16) are proportional to the factor $\sin 2\delta$. As ξ_d varies, these higher harmonics evolve continuously in the range $0 \leq 4\delta \leq 4\pi$, simultaneously with the electron filling $0 \leq N_d \leq N$. Figures 7(a)–7(f) show results for C_S , W_S , and Θ_S for $N = 4$ and 6 .

Each curve for C_S , shown in Figs. 7(a) and 7(b), exhibits two valleys situated at the valence fluctuation regions $\xi_d \simeq \pm(N-1)U/2$ for large U . These valleys rise all around as U increases. Notably, for $N = 4$, the bottom value of C_S turns positive for large interactions $U/(\pi\Delta) \gtrsim 5$, while for $N = 6$, it remains negative even for the largest interaction $U/(\pi\Delta) = 6$ examined in this study.

Near the electron-hole symmetric point $\xi_d = 0$, where $\delta = \pi/2$ and $N_d = N/2$, the two-body part W_S dominates the nonlinear noise coefficient C_S since the three-body correlations disappear around this point:

$$W_S \xrightarrow{\xi_d=0} 1 + \frac{9\tilde{K}^2}{N-1}, \quad \Theta_S \xrightarrow{\xi_d=0} 0. \quad (7.5)$$

In particular, in the limit of $U \rightarrow \infty$, the rescaled Wilson ratio approaches the saturation value $\tilde{K} \rightarrow 1$. Hence, the coefficient for the order $|eV|^3$ term reaches $(192/\pi^2)C_S \xrightarrow{\xi_d=0 \& U \rightarrow \infty} 4$ for $N = 4$, and it reaches $14/5$ for $N = 6$: the height of this ridge decreases as N

increases.

In contrast, in the opposite limit $|\xi_d| \rightarrow \infty$, both the two-body and the three-body parts approach the noninteracting values

$$W_S \xrightarrow{|\xi_d| \rightarrow \infty} 1, \quad \Theta_S \xrightarrow{|\xi_d| \rightarrow \infty} 2, \quad (7.6)$$

since $\cos 2\delta \rightarrow 1$, $\tilde{K} \rightarrow 0$, and $\Theta_I \rightarrow -2$ in this limit. Therefore, W_S and Θ_S contribute comparably to C_S in the region $|\xi_d| \gtrsim (N-1)U/2$, where the impurity levels are either almost empty $N_d \simeq 0$ or fully occupied $N_d \simeq N$. In particular, as seen in Figs. 7(c) and 7(d), the two-body part approaches the saturation value $W_S \rightarrow 1$ already at $|\xi_d| \simeq (N-1)U/2$ for large interactions $U/(\pi\Delta) \gtrsim 3$.

In the strong-coupling region $|\xi_d| \lesssim (N-1)U/2$ for large U , the behavior of two-body part W_S is determined by the higher-harmonic $\cos 4\delta$ term, as

$$W_S \simeq \frac{1}{2} \left(3 + \frac{5}{N-1} \right) + \frac{1}{2} \left(\frac{13}{N-1} - 1 \right) \cos 4\delta, \quad (7.7)$$

since the Wilson ratio is locked at $\tilde{K} \simeq 1.0$ in this region. As seen in Figs. 7(c) and 7(d), the two-body part W_S has local minima at quarter and three-quarters filling points, which occur at $\delta = \pi/4$ and $3\pi/4$, or $|\xi_d|/U \simeq N/4$ for large U . At these local minima, W_S take a positive value for $N \geq 4$, as it can be deduced from Eq. (7.7). This is in contrast to the SU(2) case where the local minima of W_S take a negative value, as shown in Appendix F. In the strong-coupling region $|\xi_d| \lesssim (N-1)U/2$, the three-body part takes the following form, for large U ,

$$\Theta_S \simeq \frac{\chi_{\sigma\sigma\sigma}^{[3]}}{2\pi \chi_{\sigma\sigma}^2} \sin 4\delta, \quad (7.8)$$

due to the property described in Eq. (6.7). Equation (7.8) clearly shows that the three-body part vanishes, $\Theta_S = 0$, at quarter $\delta = \pi/4$ and three-quarters $\delta = 3\pi/4$ fillings. Therefore, at these filling points, Θ_S does not exhibit the plateau structures for $N = 4$ in Fig. 7(e), despite the fact that Θ_V clearly exhibits the plateau structures as seen in Fig. 5(e). In contrast, for $N = 6$, Θ_S shows the clear plateau structures in Fig. 7(f) at the fillings of $N_d = 2$ and 4. The three-body parts Θ_S for both $N = 4$ and 6 cases also have pronounced local minima near the valence fluctuation regions $\xi_d \simeq \pm(N-1)U/2$, which cause the valley structure appearing in C_S . A similar valley structure also emerges in C_S for $N = 2$, as shown in Appendix F. However, it stems from the two-body correlations W_S , instead of Θ_S , in the SU(2) case.

VIII. THERMOELECTRIC TRANSPORT OF SU(4) & SU(6) QUANTUM DOTS

We next consider the order T^2 term of the linear conductance $g = dJ/dV|_{eV=0}$ and the order T^3 term of thermal conductance κ_{QD} of SU(N) quantum dots.

A. C_T : order T^2 term of dJ/dV

The coefficient C_T for the order T^2 conductance, defined in Table II, also consists of two-body parts W_T and three-body part Θ_T :

$$C_T = \frac{\pi^2}{48} (W_T + \Theta_T), \quad \Theta_T \equiv \Theta_I + \tilde{\Theta}_{\text{II}}. \quad (8.1)$$

In particular, the three-body part Θ_T is solely determined by the derivatives of the charge and spin susceptibilities, given in Eqs. (6.1) and (6.2), and does not depend on $\chi_B^{[3]}$:

$$\Theta_T = \frac{(4T^*)^2}{N} \left[\frac{\partial \bar{\chi}_C}{\partial \epsilon_d} + (N-1) \frac{\partial \bar{\chi}_S}{\partial \epsilon_d} \right] \frac{\sin 2\delta}{2\pi}. \quad (8.2)$$

This is a quite distinct characteristics of C_T from the next-leading order terms of the other transport coefficients. Figures 8(a)–8(f) show the NRG results for C_T , W_T , and Θ_T .

We see in Figs. 8(e) and 8(f) that the three-body contribution almost vanishes, $\Theta_T \simeq 0.0$, in the wide strong-coupling region $|\xi_d| \lesssim (N-1)U/2$, in which the occupation number varies with ξ_d , in the range of $1 \lesssim N_d \lesssim N-1$. This is because the magnitudes of the derivatives $\partial \bar{\chi}_C / \partial \epsilon_d$ and $\partial \bar{\chi}_S / \partial \epsilon_d$, appearing in the right-hand side of Eq. (8.2), are significantly suppressed by the Coulomb repulsion in this region, as demonstrated in Figs. 3(a)–3(d).

Therefore, the two-body part W_T dominates C_T in the strong-coupling region $|\xi_d| \lesssim (N-1)U/2$, and it takes the following form for large U ,

$$W_T \simeq \left[1 + \frac{2}{N-1} \right] (2 \sin^2 \delta - 1), \quad \Theta_T \simeq 0, \quad (8.3)$$

as the rescaled Wilson ratio reaches the saturation value $\tilde{K} \rightarrow 1$. Hence, the plateau structure of C_T is determined by the $\sin^2 \delta$ term of W_T in Eq. (8.3). In particular, the plateau around the half filling point $|\xi_d| \lesssim U/2$ reaches the height of $(48/\pi^2) C_T \xrightarrow{U \rightarrow \infty} 5/3$ and $7/5$ for $N = 4$ and 6, respectively, since $\delta \simeq \pi/2$ in this region. The order T^2 conductance, C_T , vanishes at $|\xi_d|/U \simeq N/4$, more specifically at the quarter and the three-quarter fillings where the phase shift reaches $\delta = \pi/4$ or $3\pi/4$. The zero points of C_T emerge at integer fillings in the case of $N \equiv 0 \pmod{4}$ at which the SU(N) Kondo effect is occurring, whereas for $N \equiv 2 \pmod{4}$ the zeros emerge at half-integer fillings in between the two adjacent Kondo states. This explains the reason why the SU(4) Kondo state at quarter filling exhibits universal T/T^* -scaling behavior, which shows the $(T/T^*)^4$ dependence at low temperatures instead of the $(T/T^*)^2$ dependence [68].

In the valence fluctuation and empty (or fully-occupied) orbital regimes, which spread over the regions of $|\xi_d| \gtrsim (N-1)U/2$, the three-body part Θ_T becomes comparable to the two-body part W_T . Both of these

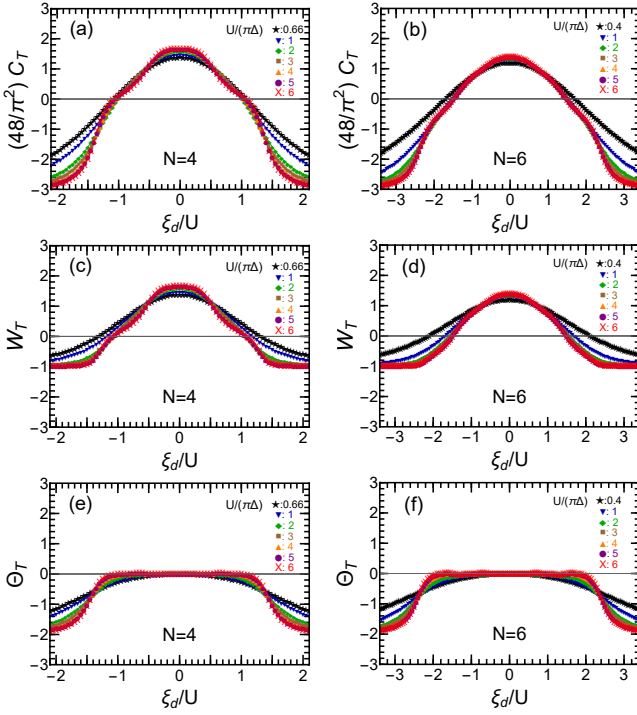


FIG. 8. ξ_d dependence of $C_T = (\pi^2/48)(W_T + \Theta_T)$, two-body part W_T , and three-body part $\Theta_T \equiv \Theta_I + 3\Theta_{II}$. Left panels: $N = 4$, for $U/(\pi\Delta) = 2/3(\star)$, 1(\blacktriangledown), 2(\blacklozenge), 3(\blacksquare), 4(\blacktriangle), 5(\bullet), 6(\times). Right panels: $N = 6$, for $U/(\pi\Delta) = 2/5(\star)$, 1(\blacktriangledown), 2(\blacklozenge), 3(\blacksquare), 4(\blacktriangle), 5(\bullet), 6(\times).

parts approach the noninteracting values in the limit of $|\xi_d| \rightarrow \infty$:

$$W_T \xrightarrow{|\xi_d| \rightarrow \infty} -1, \quad \Theta_T \xrightarrow{|\xi_d| \rightarrow \infty} -2. \quad (8.4)$$

B. C_κ^{QD} : order T^3 term of κ_{QD}

The coefficient C_κ^{QD} for the order T^3 term of the thermal conductance κ_{QD} can also be decomposed into two parts, W_κ^{QD} and $\Theta_\kappa^{\text{QD}}$, as shown in Table II:

$$C_\kappa^{\text{QD}} = \frac{7\pi^2}{80} (W_\kappa^{\text{QD}} + \Theta_\kappa^{\text{QD}}), \quad \Theta_\kappa^{\text{QD}} \equiv \Theta_I + \frac{5}{21}\tilde{\Theta}_{II}. \quad (8.5)$$

In contrast to Θ_T of the conductance given in Eq. (8.2), the three-body part $\Theta_\kappa^{\text{QD}}$ of the thermal conductance depends on $\chi_B^{[3]}$ as well as $\partial\bar{\chi}_C/\partial\epsilon_d$ and $\partial\bar{\chi}_S/\partial\epsilon_d$. The contribution of $\chi_B^{[3]}$ enters through $\chi_{\sigma\sigma\sigma}^{[3]}$ and $\tilde{\chi}_{\sigma\sigma'\sigma'}^{[3]}$, described in Eqs. (5.10) and (5.11). This component $\chi_B^{[3]}$ yields the plateau structure in $\Theta_\kappa^{\text{QD}}$, which reflects the staircase behavior seen in Figs. 3(e) and 3(f). Figure 9 shows the NRG results for C_κ^{QD} , W_κ^{QD} , and $\Theta_\kappa^{\text{QD}}$ in the SU(4) and SU(6) cases.

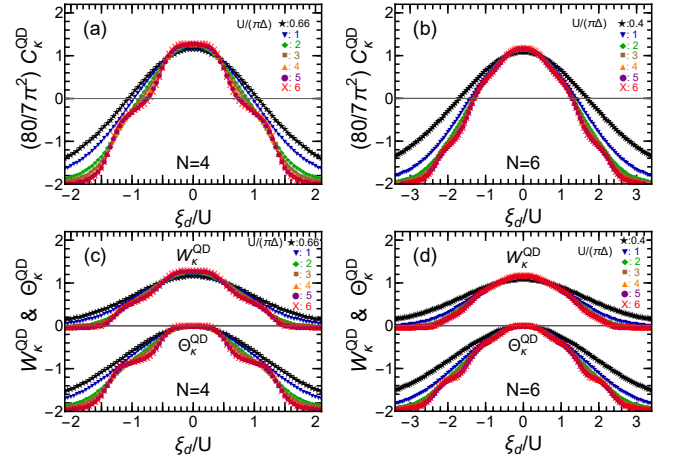


FIG. 9. ξ_d dependence of $C_\kappa^{\text{QD}} = (7\pi^2/80)(W_\kappa^{\text{QD}} + \Theta_\kappa^{\text{QD}})$, two-body part W_κ^{QD} , and three-body part $\Theta_\kappa^{\text{QD}} = \Theta_I + \frac{5}{21}\Theta_{II}$. Left panels: $N = 4$, for $U/(\pi\Delta) = 2/3(\star)$, 1(\blacktriangledown), 2(\blacklozenge), 3(\blacksquare), 4(\blacktriangle), 5(\bullet), 6(\times). Right panels: $N = 6$, for $U/(\pi\Delta) = 2/5(\star)$, 1(\blacktriangledown), 2(\blacklozenge), 3(\blacksquare), 4(\blacktriangle), 5(\bullet), 6(\times).

Near half filling in the region of $|\xi_d| \lesssim U/2$, the two-body part W_κ^{QD} dominates C_κ^{QD} as the three-body part $\Theta_\kappa^{\text{QD}}$ disappears near half filling $\xi_d = 0$, i.e., $\delta = \pi/2$:

$$W_\kappa^{\text{QD}} \xrightarrow{\xi_d=0} 1 + \frac{6\tilde{K}^2}{7(N-1)}, \quad \Theta_\kappa^{\text{QD}} \xrightarrow{\xi_d=0} 0. \quad (8.6)$$

In particular, in the strong interaction limit $U \rightarrow \infty$, the coefficient C_κ^{QD} for $N = 4$ and 6 approach the values of $[80/(7\pi^2)]C_\kappa^{\text{QD}} \xrightarrow{\xi_d=0 \& U \rightarrow \infty} 9/7$ and $41/35$, respectively.

The rescaled Wilson ratio takes the values very close to the saturation value $\tilde{K} \rightarrow 1$ for large U in the strong-coupling region of $|\xi_d| \lesssim (N-1)U/2$, as described in Appendix E. Similarly, in this region, the three-body correlations show the property described in Eq. (6.7), and thus W_κ^{QD} and $\Theta_\kappa^{\text{QD}}$ take the form

$$W_\kappa^{\text{QD}} \simeq \frac{1}{21} \left[10 + \left(11 + \frac{18}{N-1} \right) (2\sin^2 \delta - 1) \right],$$

$$\Theta_\kappa^{\text{QD}} \simeq \frac{16}{21} \Theta_I. \quad (8.7)$$

Therefore, the plateau structure of W_κ^{QD} is determined by the $\sin^2 \delta$ term appearing in the right-hand side, while the structure of $\Theta_\kappa^{\text{QD}}$ reflects the behavior of Θ_I shown in Fig. 4(e) and 4(f). The coefficient C_κ^{QD} changes sign in the strong-coupling region at two points of ξ_d , which are incommensurate with the occupation number N_d in contrast to C_T that changes sign at 1/4 and 3/4 fillings.

In the opposite limit $|\xi_d| \rightarrow \infty$, both the two-body and three-body parts approach the noninteracting values,

$$W_\kappa^{\text{QD}} \xrightarrow{|\xi_d| \rightarrow \infty} -\frac{1}{21}, \quad \Theta_\kappa^{\text{QD}} \xrightarrow{|\xi_d| \rightarrow \infty} -2. \quad (8.8)$$

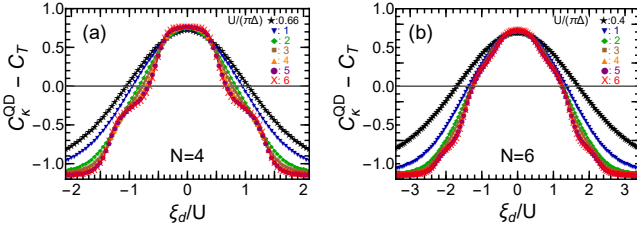


FIG. 10. Order T^2 term $C_L^{\text{QD}} = C_k^{\text{QD}} - C_T$ of Lorenz number L_{QD} is plotted vs ξ_d . Left panel: $N = 4$, for $U/(\pi\Delta) = 2/3$ (\star), 1 (\blacktriangledown), 2 (\blacklozenge), 3 (\blacksquare), 4 (\blacktriangle), 5 (\bullet), 6 (\times). Right panel: $N = 6$, for $U/(\pi\Delta) = 2/5$ (\star), 1 (\blacktriangledown), 2 (\blacklozenge), 3 (\blacksquare), 4 (\blacktriangle), 5 (\bullet), 6 (\times).

C. C_L^{QD} : order T^2 term of L_{QD}

The Lorenz number $L_{\text{QD}} \equiv \kappa_{\text{QD}}/(gT)$ for quantum dots is defined as the ratio of the thermal conductance κ_{QD}/T to the electrical conductance g . It takes the universal Wiedemann-Franz value at zero temperature: $L_{\text{QD}} \xrightarrow{T \rightarrow 0} \pi^2/(3e^2)$. However, as the temperature rises, it deviates from the universal value, showing the T^2 dependence described in Tables I and II. The coefficient for the order T^2 term is given by $C_L^{\text{QD}} = C_k^{\text{QD}} - C_T$, as a difference between the next-leading order terms of κ_{QD}/T and g .

Figure 10(a) and 10(b) show the NRG results for C_L^{QD} in the SU(4) and SU(6) cases, respectively. Near half filling $|\xi_d| \lesssim U/2$, the coefficient C_L^{QD} is determined by the two-body part W_L^{QD} as the three-body part $\Theta_L^{\text{QD}} \equiv 16\Theta_1$ vanishes at $\xi_d = 0$, as seen in Fig. 4(e) and 4(f):

$$C_L^{\text{QD}} \xrightarrow{\xi_d=0} \frac{\pi^2}{30} \left(2 + \frac{\tilde{K}^2}{N-1} \right) > 0. \quad (8.9)$$

It takes a positive value and reaches $C_L^{\text{QD}} \xrightarrow{\xi_d=0 \& U=\infty} 0,767\dots$ for $N = 4$, and $0.723\dots$ for $N = 6$, in the limit of $U \rightarrow \infty$ where $\tilde{K} \rightarrow 1$.

In the strong-coupling region $|\xi_d| \lesssim (N-1)U/2$, the coefficient C_L^{QD} exhibits the plateau structures for large U , reflecting the corresponding structures of C_T and C_k^{QD} . The coefficient C_L^{QD} changes sign at the points where the order T^2 terms of κ_{QD}/T and g coincide, i.e., $C_k^{\text{QD}} = C_T$.

In the other regions at $|\xi_d| \gtrsim (N-1)U/2$, the impurity levels approach the empty state $N_d \simeq 0$ or fully occupied $N_d \simeq N$ state. In particular, in the limit of $|\xi_d| \rightarrow \infty$, both the two-body and three-body parts approach the noninteracting values, $W_L^{\text{QD}} \xrightarrow{|\xi_d| \rightarrow \infty} 4$ and $16\Theta_1 \xrightarrow{|\xi_d| \rightarrow \infty} -32$, and thus

$$C_L^{\text{QD}} \xrightarrow{|\xi_d| \rightarrow \infty} -\frac{7\pi^2}{60} = -1.151\dots < 0. \quad (8.10)$$

IX. FERMILY LIQUID DESCRIPTION FOR

SU(N) SYMMETRIC MAGNETIC ALLOYS

We have discussed, in the previous sections, low-energy transport properties of SU(N) quantum dots, by extending the Fermi liquid description to the next-leading order terms which contribute to the transport at finite temperatures or at finite bias voltages. Our formulation is applicable to a wide class of Kondo systems other than quantum dots, particularly to dilute magnetic alloys (MA) composed of $3d$, $4f$, or $5f$ electrons [2]. In this and the next sections, we apply this formulation to dilute magnetic alloys away from half filling, taking into account exactly the order ω^2 and T^2 energy shifts of quasiparticles that enter through the real part of the self-energy $\Sigma_\sigma^r(\omega)$ given in Appendix B.

The thermoelectric transport coefficients of magnetic alloys in the linear-response regime can be derived from the function $\mathcal{L}_{n,\sigma}^{\text{MA}}$ for $n = 0, 1$, and 2 , defined by [43]

$$\mathcal{L}_{n,\sigma}^{\text{MA}} = \int_{-\infty}^{\infty} d\omega \frac{\omega^n}{\pi \Delta A_\sigma(\omega)} \left(-\frac{\partial f(\omega)}{\partial \omega} \right). \quad (9.1)$$

Here, the inverse spectral function $1/A_\sigma(\omega)$ in the integrand represents the relaxation time of conduction electrons, which depends on T as well as ω . The low-temperature expansion of $\mathcal{L}_{n,\sigma}^{\text{MA}}$ can be deduced from the exact low-energy asymptotic of $1/A_\sigma(\omega)$, given in Appendix B. We have presented the expansion formulas for the standard $N = 2$ Anderson impurity model in a previous paper [21]. In this work, we extend the formulation to multi-level impurities in a general form without assuming the SU(N) symmetry. Details of the derivation are given in Appendix G.

In the following, we consider the behavior of the next-leading order terms of electrical conductivity σ_{MA} and thermal conductivity κ_{MA} of magnetic alloys in the SU(N) symmetric case, where $\epsilon_{d\sigma} \equiv \epsilon_d$ for all σ , and $U_{\sigma\sigma'} \equiv U$ for all σ and σ' . In this case, the formulas given in Appendix G are simplified, and as a result, the electrical resistivity $\varrho_{\text{MA}} = 1/\sigma_{\text{MA}}$, the thermal resistivity $1/\kappa_{\text{MA}}$, and the Lorenz number $L_{\text{MA}} = \kappa_{\text{MA}}/(\sigma_{\text{MA}} T)$ can be expressed in the form,

$$\varrho_{\text{MA}} = \frac{1}{\sigma_{\text{MA}}^{\text{unit}}} \left[\sin^2 \delta - C_\rho^{\text{MA}} \left(\frac{\pi T}{T^*} \right)^2 + \dots \right], \quad (9.2)$$

$$\frac{1}{\kappa_{\text{MA}}} = \frac{3e^2}{\pi^2 \sigma_{\text{MA}}^{\text{unit}} T} \left[\sin^2 \delta - C_\kappa^{\text{MA}} \left(\frac{\pi T}{T^*} \right)^2 + \dots \right], \quad (9.3)$$

$$L_{\text{MA}} = \frac{\pi^2}{3e^2} \left[1 - \frac{C_L^{\text{MA}}}{\sin^2 \delta} \left(\frac{\pi T}{T^*} \right)^2 + \dots \right]. \quad (9.4)$$

Here, $\sigma_{\text{MA}}^{\text{unit}}$ is the unitary-limit value of electrical conductivity. The explicit expressions of the dimensionless coefficients C_ρ^{MA} , C_κ^{MA} , and C_L^{MA} are listed in Table II. These coefficients C 's for magnetic alloys can also be decomposed into the two-body W part and the three-body

Θ part, as those for quantum dots. Note that the following relations hold between the coefficients for magnetic alloys and quantum dots:

$$C_\rho^{\text{MA}} = \frac{\pi^2}{12} \cos^2 \delta + C_T, \quad (9.5)$$

$$C_\kappa^{\text{MA}} = \frac{11\pi^2}{60} \cos^2 \delta + C_\kappa^{\text{QD}}, \quad (9.6)$$

$$C_L^{\text{MA}} = -\frac{\pi^2}{10} \cos^2 \delta - C_L^{\text{QD}}. \quad (9.7)$$

In particular, the $\cos^2 \delta$ term appearing in the right-hand side vanishes at half filling, i.e., $\delta = \pi/2$. In this case the coefficients for magnetic alloys in the left-hand side coincide with their quantum-dot counterparts in the right-hand side, except for the signs of C_L^{MA} and C_L^{QD} . The behavior of these coefficients for magnetic alloys also reflects the properties of low-lying energy states and significantly depends on the occupation number N_d and the interaction strength U .

X. THERMOELECTRIC TRANSPORT OF SU(4) & SU(6) MAGNETIC ALLOYS

We consider here the next-leading order terms of the electrical resistivity ϱ_{MA} and thermal resistivity $1/\kappa_{\text{MA}}$ of SU(N) symmetric magnetic alloys for $N = 4$ and 6. For comparison, we also provide the NRG results for these transport coefficients in the SU(2) case in Appendix F, and the analytic expressions of C 's for noninteracting magnetic alloys in Appendix H.

A. C_ρ^{MA} : order T^2 term of ϱ_{MA}

The coefficient C_ρ^{MA} for the order T^2 resistivity, is defined in Table II. It consists of two-body part W_ρ^{MA} and three-body part Θ_ρ^{MA} :

$$C_\rho^{\text{MA}} = \frac{\pi^2}{48} (W_\rho^{\text{MA}} + \Theta_\rho^{\text{MA}}), \quad \Theta_\rho^{\text{MA}} \equiv \Theta_{\text{I}} + \tilde{\Theta}_{\text{II}}. \quad (10.1)$$

Note that $\Theta_\rho^{\text{MA}} \equiv \Theta_T$, i.e., the three-body part for the T^2 resistivity of magnetic alloys is identical to the one for the T^2 conductance of quantum dots. Therefore, Θ_ρ^{MA} does not depend on $\chi_B^{[3]}$ and is determined by the derivative of the charge and spin susceptibilities through Eq. (8.2). Figures 11(a)–11(d) show the NRG results for C_ρ^{MA} , W_ρ^{MA} , and Θ_ρ^{MA} for both the SU(4) and SU(6) symmetric cases.

The coefficient C_ρ^{MA} is positive and is less sensitive to the impurity level position ξ_d as compared to the quantum-dot counterpart C_T shown in Fig. 8. This difference is caused by the first term, $(\pi^2/12) \cos^2 \delta$, appearing in the right-hand side of Eq. (9.5). In particular, in the noninteracting case, it becomes a constant,

$(48/\pi^2)C_\rho^{\text{MA}} \xrightarrow{U=0} 1$, independent of the level position, as all effects due to ϵ_d are absorbed into the characteristic energy T^* for $U = 0$ (see Appendix H). Therefore, it is the strong electron correlation that makes C_ρ^{MA} , shown in Figs. 11(a) and 11(b), deviates from the constant value.

The three-body part almost vanishes, $\Theta_\rho^{\text{MA}} \simeq 0$, for large U in the strong-coupling region $|\xi_d| \lesssim (N-1)U/2$, as mentioned for Θ_T in Eq. (8.2). This is caused by the fact that the magnitudes of the derivatives, $\partial \bar{\chi}_C / \partial \epsilon_d$ and $\partial \bar{\chi}_S / \partial \epsilon_d$, are significantly suppressed by the Coulomb repulsion in the wide range of electron filling $1 \lesssim N_d \lesssim N-1$, as demonstrated in Figs. 3(a)–3(d). Therefore, in this region $|\xi_d| \lesssim (N-1)U/2$, the coefficient C_ρ^{MA} is determined solely by the two-body part W_ρ^{MA} , which takes the form

$$C_\rho^{\text{MA}} \simeq \frac{\pi^2}{48} \left[2 + \left(1 - \frac{2}{N-1} \right) (1 - 2 \sin^2 \delta) \right] > 0, \quad (10.2)$$

as the rescaled Wilson ratio is saturated to $\tilde{K} \simeq 1$. Hence, the plateaus emerging around the integer filling points $\delta/\pi = 1, 2, \dots, N-1$, reflect the structures of the Kondo ridge occurring for the transmission probability $\sin^2 \delta$, seen in Figs. 15(b) and 16(b) in Appendix E. Among these plateaus, the one at half filling, where $\delta = \pi/2$, takes the smallest value:

$(48/\pi^2)C_\rho^{\text{MA}} \xrightarrow{\xi_d=0 \& U \rightarrow \infty} 5/3$ and $7/5$ for $N = 4$ and 6, respectively. As ξ_d moves away from half filling, the coefficient C_ρ^{MA} increases in the region of $|\xi_d| \lesssim (N-1)U/2$. Equation (10.2) also indicates that the plateau becomes highest at the electron fillings of $N_d \simeq 1$ and $N-1$:

$(48/\pi^2)C_\rho^{\text{MA}} \xrightarrow{U \rightarrow \infty, \delta = \pi/N} 2$ and $23/10$ for $N = 4$ and 6, respectively. The NRG results for C_ρ^{MA} , shown in Figs. 11(a) and 11(b), clearly demonstrate these behaviors, which are quite different from the behaviors of C_T of quantum dots. Equation (10.2) also shows that, in the SU(2) symmetric case where $N = 2$, the coefficient C_ρ^{MA} takes the maximum value at half filling, as demonstrated also in Appendix F.

In contrast, at $|\xi_d| \gtrsim (N-1)U/2$, the occupation number approaches the empty $N_d \simeq 0$ or the fully occupied $N_d \simeq N$ states as the impurity level moves further away from the Fermi level. In this region, both the two-body W_ρ^{MA} and three-body Θ_ρ^{MA} parts give comparable contributions to C_ρ^{MA} , and approach the noninteracting values:

$$W_\rho^{\text{MA}} \xrightarrow{|\xi_d| \rightarrow \infty} 3, \quad \Theta_\rho^{\text{MA}} \xrightarrow{|\xi_d| \rightarrow \infty} -2, \quad (10.3)$$

and thus $(48/\pi^2)C_\rho^{\text{MA}} \xrightarrow{|\xi_d| \rightarrow \infty} 1$.

B. C_κ^{MA} : order T^3 term of κ_{MA}

We next consider the order T^3 term of thermal conductivity κ_{MA} of the SU(N) symmetric magnetic alloys.

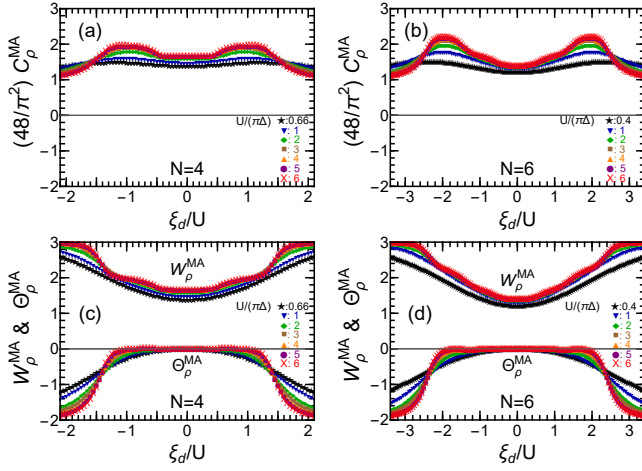


FIG. 11. ξ_d dependence of $C_\rho^{\text{MA}} = (\pi^2/48)(W_\rho^{\text{MA}} + \Theta_\rho^{\text{MA}})$, two-body part W_ρ^{MA} , and three-body part $\Theta_\rho^{\text{MA}} = \Theta_I + \tilde{\Theta}_{\text{II}}$. Left panels: $N = 4$, for $U/(\pi\Delta) = 2/3$ (\star), 1(\blacktriangledown), 2(\blacklozenge), 3(\blacksquare), 4(\blacktriangle), 5(\bullet), 6(\times). Right panels: $N = 6$, for $U/(\pi\Delta) = 2/5$ (\star), 1(\blacktriangledown), 2(\blacklozenge), 3(\blacktriangle), 4(\blacktriangle), 5(\bullet), 6(\times).

The coefficient C_κ^{MA} , defined in Tables I and II, consists of two-body W_κ^{MA} and three-body $\Theta_\kappa^{\text{MA}}$ parts:

$$C_\kappa^{\text{MA}} = \frac{7\pi^2}{80} (W_\kappa^{\text{MA}} + \Theta_\kappa^{\text{MA}}), \quad \Theta_\kappa^{\text{MA}} \equiv \Theta_I + \frac{5}{21}\tilde{\Theta}_{\text{II}}. \quad (10.4)$$

Note that $\Theta_\kappa^{\text{MA}} \equiv \Theta_\kappa^{\text{QD}}$, i.e., the three-body part for C_κ^{MA} of magnetic alloys is identical to the one for the T^3 thermal conductance of quantum dots. The NRG results for these coefficients C_κ^{MA} , W_κ^{MA} , and $\Theta_\kappa^{\text{MA}}$ are shown in Figs. 12(a)–12(d) for $N = 4$ and 6.

The coefficient C_κ^{MA} for magnetic alloys is less sensitive to ξ_d as compared to C_κ^{QD} for quantum dots. This difference is caused by the contribution of the first term, $(11\pi^2/60)\cos^2\delta$, in the right-hand side of Eq. (9.6). The coefficient C_κ^{MA} is positive and has a broad peak at $\xi_d = 0$, the height of which is determined by the two-body contribution W_κ^{MA} as three-body part $\Theta_\kappa^{\text{MA}}$ vanishes in the electron-hole symmetric case:

$$W_\kappa^{\text{MA}} \xrightarrow{\xi_d=0} 1 + \frac{6\tilde{K}^2}{7(N-1)}, \quad \Theta_\kappa^{\text{MA}} \xrightarrow{\xi_d=0} 0. \quad (10.5)$$

In the limit of $U \rightarrow \infty$, it reaches the maximum possible value, $[80/(7\pi^2)]C_\kappa^{\text{MA}} \xrightarrow{\xi_d=0 \& U \rightarrow \infty} 9/7$ and $41/35$ for $N = 4$ and 6, respectively.

In the strong-coupling region $|\xi_d| \lesssim (N-1)U/2$, the coefficient C_κ^{MA} takes the following form for large U ,

$$C_\kappa^{\text{MA}} \simeq \frac{\pi^2}{240} \left[32 + \left(11 - \frac{18}{N-1} \right) \cos 2\delta + 16\Theta_I \right]. \quad (10.6)$$

This is because, in this region, the rescaled Wilson ratio is almost saturated $\tilde{K} \simeq 1$ (see Appendix E) and the

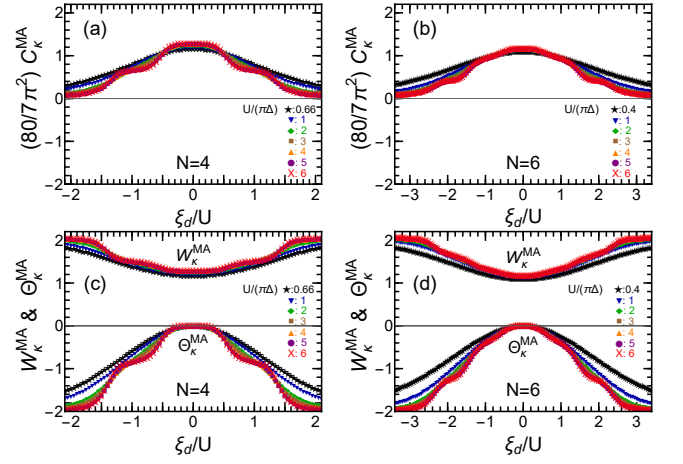


FIG. 12. ξ_d dependence of $C_\kappa^{\text{MA}} = (7\pi^2/80)(W_\kappa^{\text{MA}} + \Theta_\kappa^{\text{MA}})$, two-body part W_κ^{MA} , and three-body part $\Theta_\kappa^{\text{MA}} = \Theta_I + \frac{5}{21}\tilde{\Theta}_{\text{II}}$. Left panels: $N = 4$, for $U/(\pi\Delta) = 2/3$ (\star), 1(\blacktriangledown), 2(\blacklozenge), 3(\blacksquare), 4(\blacktriangle), 5(\bullet), 6(\times). Right panels: $N = 6$, for $U/(\pi\Delta) = 2/5$ (\star), 1(\blacktriangledown), 2(\blacklozenge), 3(\blacktriangle), 4(\blacktriangle), 5(\bullet), 6(\times).

three-body part is parameterized by a single component, $\Theta_\kappa^{\text{MA}} \simeq \frac{16}{21}\Theta_I$, due to the property described in Eq. (6.7). The plateau structures of C_κ^{MA} , appearing in Figs. 12(a) and 12(b) around the integer filling points $N_d = 1, 2, \dots, N-1$, are determined by both the $\cos 2\delta$ term in W_κ^{MA} and the plateaus occurring in $\Theta_\kappa^{\text{MA}}$ seen in Figs. 12(c) and 12(d).

In contrast, at $|\xi_d| \gtrsim (N-1)U/2$, the electron filling approaches the empty $N_d \simeq 0$ or the fully occupied $N_d \simeq N$ states as the impurity level goes very far away from the half filled point. Therefore, the order T^3 thermal conductivity for magnetic alloys also approaches the noninteracting value in this limit:

$$W_\kappa^{\text{MA}} \xrightarrow{|\xi_d| \rightarrow \infty} \frac{43}{21}, \quad \Theta_\kappa^{\text{MA}} \xrightarrow{|\xi_d| \rightarrow \infty} -2, \quad (10.7)$$

and thus $[80/(7\pi^2)]C_\kappa^{\text{MA}} \xrightarrow{|\xi_d| \rightarrow \infty} 1/21$.

C. C_L^{MA} : order T^2 term of L_{MA}

The Lorenz number $L_{\text{MA}} \equiv \kappa_{\text{MA}}/(\sigma_{\text{MA}}T)$ for magnetic alloys is defined as the ratio of the thermal conductivity κ_{MA}/T to electrical conductivity σ_{MA} . It takes the universal Wiedemann-Franz value at zero temperature: $L_{\text{MA}} \xrightarrow{T \rightarrow 0} \pi^2/(3e^2)$. However, it deviates from this value as the temperature increases, showing the T^2 dependence as described in Eq. (9.4). The precise expansion formula for the coefficient C_L^{MA} for the order T^2 term is shown in Table II. It is given by the difference, $C_L^{\text{MA}} = C_\rho^{\text{MA}} - C_\kappa^{\text{MA}}$, between the order T^2 term of the resistivities, $1/\sigma_{\text{MA}}$ and T/κ_{MA} , defined in Eqs. (9.2) and (9.4). The coefficient C_L^{MA} for magnetic alloys and the quantum-dot counterpart C_L^{QM} are related to each other

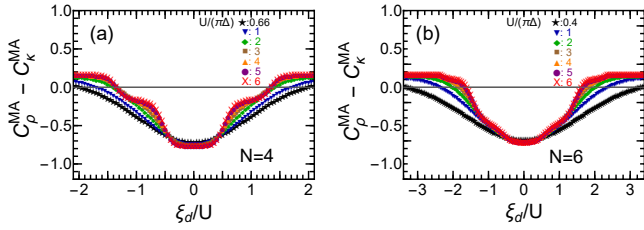


FIG. 13. Order T^2 term $C_L^{\text{MA}} = C_\rho^{\text{MA}} - C_\kappa^{\text{MA}}$ of Lorenz number L_{MA} is plotted vs ξ_d . Left panel: $N = 4$, for $U/(\pi\Delta) = 2/3$ (\star), 1 (\blacktriangledown), 2 (\blacklozenge), 3 (\blacksquare), 4 (\blacktriangle), 5 (\bullet), 6 (\times). Right panel: $N = 6$, for $U/(\pi\Delta) = 2/5$ (\star), 1 (\blacktriangledown), 2 (\blacklozenge), 3 (\blacksquare), 4 (\blacktriangle), 5 (\bullet), 6 (\times).

through Eq. (9.7): these two coefficients tend to have opposite signs. In Appendix H, we have also provide an analytic formula for C_L^{MA} in the noninteraction case, for comparison.

The NRG results for C_L^{MA} are shown in Figs. 13(a) and 13(b) for $N = 4$ and 6 , respectively. Near half filling $|\xi_d| \lesssim U/2$, the coefficient C_L^{MA} is determined by the two-body part W_L^{MA} as the three-body part, given by $-16\Theta_1$, vanishes at $\xi_d = 0$:

$$C_L^{\text{MA}} \xrightarrow{\xi_d=0} -\frac{\pi^2}{30} \left(2 + \frac{\tilde{K}^2}{N-1} \right) < 0. \quad (10.8)$$

This coefficient attains its greatest possible negative value in the limit of $U \rightarrow \infty$ where $\tilde{K} \rightarrow 1$: $C_L^{\text{MA}} \xrightarrow{\xi_d=0 \text{ \& } U \rightarrow \infty} -0,767 \dots$ for $N = 4$, and $-0.723 \dots$ for $N = 6$.

In the strong-coupling region $|\xi_d| \lesssim (N-1)U/2$, the C_L^{MA} also exhibits the plateau structures around the integer filling points $\xi_d/U = 0, \pm 1, \dots, \pm(N-2)/2$ for large U , reflecting the structures that appear for both C_ρ^{MA} and C_κ^{MA} . In particular, the plateaus at $N_d \simeq \frac{N}{2} \pm 1$ fillings, seen in Figs. 13(a) and 13(b) for $U/(\pi\Delta) \gtrsim 3$, take a negative value for both $N = 4$ and $N = 6$, whereas the other plateaus become positive for $N = 6$ as the electrical resistivity dominates, i.e., $C_\rho^{\text{MA}} > C_\kappa^{\text{MA}}$.

As the impurity level goes far away from the Fermi level in the region $|\xi_d| \gtrsim (N-1)U/2$, the occupation number approaches $N_d \simeq 0$ or $N_d \simeq N$. In the limit of $|\xi_d| \rightarrow \infty$, the two-body and three-body parts take the noninteracting values, $W_L^{\text{MA}} \xrightarrow{|\xi_d| \rightarrow \infty} -28$ and $-16\Theta_1 \xrightarrow{|\xi_d| \rightarrow \infty} 32$, and the coefficient C_L^{MA} converges to the positive value,

$$C_L^{\text{MA}} \xrightarrow{|\xi_d| \rightarrow \infty} \frac{\pi^2}{60} = 0.164 \dots > 0. \quad (10.9)$$

XI. SUMMARY

We have presented a comprehensive Fermi liquid description for nonlinear current and thermoelectric transport through quantum dots and magnetic alloys, which

is asymptotically exact at low energies up to the next-leading order terms. Our formulation is based on the multilevel Anderson model and is applicable to arbitrary impurity-level structures $\epsilon_{d\sigma}$ for $\sigma = 1, 2, \dots, N$, including the spin degrees of freedom. The coefficients for the next-leading order terms have been shown to be expressed in terms of a set of the correlation functions defined with respect to the equilibrium ground state: the phase shift δ_σ , the static susceptibilities $\chi_{\sigma_1, \sigma_2}$, and the three-body correlations $\chi_{\sigma_1, \sigma_2, \sigma_3}^{[3]}$ which emerge when the system does not have both the electron-hole and time-reversal symmetries.

Extending Yamada-Yosida's field-theoretical approach, we have obtained the formulas for the differential conductance dI/dV , current noise $S_{\text{noise}}^{\text{QD}}$ and thermal conductance κ_{QD} of quantum dots, and also the electrical resistivity ϱ_{MA} and thermal conductivity κ_{MA} of dilute magnetic alloys. In the $SU(N)$ symmetric case, these transport coefficients take simplified forms, as listed in Tables I and II, and the three-body correlations can be deduced from the derivatives of the susceptibilities: $\partial\bar{\chi}_C/\partial\epsilon_d$, $\partial\bar{\chi}_S/\partial\epsilon_d$, and $\chi_B^{[3]}$ through Eqs. (5.10)–(5.13).

We have also calculated the correlation functions for the $SU(4)$ and $SU(6)$ cases, using the NRG approach over the whole region of impurity-electron fillings N_d , which includes the Kondo and the valence-fluctuation regimes. In the $SU(N)$ case, the three-body correlations have three linearly independent components that approach each other closely as the Coulomb interaction U increases: $\chi_{\sigma\sigma\sigma}^{[3]} \simeq -(N-1)\chi_{\sigma\sigma'\sigma'}^{[3]} \simeq \frac{(N-1)(N-2)}{2}\chi_{\sigma\sigma'\sigma''}^{[3]}$ for $\sigma \neq \sigma' \neq \sigma'' \neq \sigma$, in a wide filling range $1 \lesssim N_d \lesssim N-1$. This is caused by the suppression of the derivatives of the charge and spin susceptibilities, occurring at large U : $|\partial\bar{\chi}_C/\partial\epsilon_d| \ll (T^*)^{-2}$ and $|\partial\bar{\chi}_S/\partial\epsilon_d| \ll (T^*)^{-2}$, with $T^* \equiv 1/(4\chi_{\sigma\sigma})$ the characteristic energy scale of the $SU(N)$ Fermi liquid. This property of three-body correlations is also related to a similar property of linear susceptibilities, $\chi_{\sigma\sigma} \simeq -(N-1)\chi_{\sigma\sigma'}$, which reflects the suppression of charge fluctuations, $\bar{\chi}_C \simeq 0$, occurring at large U .

The coefficients C 's for the next-leading order terms can be decomposed into the two-body part W 's and the three-body part Θ 's, as listed in Table II. The NRG results show that the three-body part Θ_V of the coefficient C_V for the order $(eV)^2$ term of dI/dV exhibits Kondo plateau structures at integer filling points $N_d = 1, 2, \dots, N-1$ for large U . These plateaus of Θ_V complement the two body part W_V , which decreases away from half filling, to form a wide ridge structure in C_V that spreads over the region of $1 \lesssim N_d \lesssim N-1$.

The linear-response term of current noise $S_{\text{noise}}^{\text{QD}}$ is maximized at quarter filling $N_d/N = 1/4$ and three-quarters $3/4$ filling, and the peaks exhibit flat structures for $N = 4$, while they are round for $N = 6$. This difference is caused by the fact that, at these fillings, the $SU(N)$ Kondo effects occur for $N \equiv 0 \pmod{4}$, while the intermediate valence fluctuations occur for $N \equiv 2$

(mod 4). The coefficient C_S for the order $|eV|^3$ nonlinear term of $S_{\text{noise}}^{\text{QD}}$ has a peak at half filling, which evolves into a plateau as U increases. As the impurity level ξ_d deviates from the half filling point, C_S decreases rapidly for $N = 4$, whereas it varies more modestly for $N = 6$. This is mainly due to the higher-harmonic “sin 4δ ” dependence of the three-body part Θ_S , which vanishes at the quarter and three-quarters filling points. As $|\xi_d|$ increases further, Θ_S has a pronounced negative minimum in the valence fluctuation regions at $\xi_d \simeq \pm(N-1)U/2$ for both $N = 4$ and 6, which yield the valley structures appearing in C_S . This is in marked contrast to the SU(2) case, where the valley structure emerging in C_S is caused by the two-body contributions W_S , instead of Θ_S .

We have also studied the coefficient C_T for the order T^2 term of the linear conductance $g \equiv dJ/dV|_{eV=0}$ and the coefficient C_κ^{QD} for the order T^3 term of thermal conductance κ_{QD} , for SU(N) quantum dots. The three-body part Θ_T of C_T is determined solely by the derivatives of charge and spin susceptibilities, i.e., $\partial\bar{\chi}_C/\partial\epsilon_d$ and $\partial\bar{\chi}_S/\partial\epsilon_d$, and is independent of $\chi_B^{[3]}$. Therefore, Θ_T is significantly suppressed and almost vanishes for strong interactions U in a wide range of the electron filling $1 \lesssim N_d \lesssim N-1$. In contrast, the three-body part $\Theta_\kappa^{\text{QD}}$ for thermal conductance involves $\chi_B^{[3]}$ and becomes comparable to the two-body part W_κ^{QD} , except for the plateau region near half filling. The Lorenz number $L_{\text{QD}} \equiv \kappa_{\text{QD}}/(gT)$ for quantum dots takes the universal Wiedemann-Franz value $\pi^2/(3e^2)$ at $T = 0$ and shows a T^2 dependence at low temperatures. The coefficient for the order T^2 term of L_{QD} is given by $C_L^{\text{QD}} = C_\kappa^{\text{QD}} - C_T$, i.e., the difference between the next-leading order terms of κ_{QD} and g . This coefficient C_L^{QD} also exhibits the Kondo plateau structures at integer filling points $N_d = 1, 2, \dots, N-1$.

The three-body correlations also play a significant role in the low-energy transport of magnetic alloys. We have investigated the behaviors of the coefficient C_ρ^{MA} for the order T^2 resistivity ρ_{MA} and C_κ^{MA} for the order T^3 thermal conductivity κ_{MA} . In the SU(N) symmetric case, the three-body parts of these coefficients become identical to the related ones for quantum dots, i.e., $\Theta_\rho^{\text{MA}} \equiv \Theta_T$ and $\Theta_\kappa^{\text{MA}} \equiv \Theta_\kappa^{\text{QD}}$. Therefore, the difference between the coefficients for MA and that for the QD counterparts arises from the two-body parts, more specifically, from the additional $\cos^2\delta$ terms appearing in the right-hand side of Eqs. (9.5) and (9.6). The additional $\cos^2\delta$ terms make the coefficients C_ρ^{MA} and C_κ^{MA} positive definite and less sensitive to the impurity level position ξ_d , compared to the QD counterparts C_T and C_κ^{QD} . The coefficient C_ρ^{MA} takes the maximum value at the electron fillings of $N_d \simeq 1$ and $N-1$ for $N \geq 4$, while in the SU(2) case C_ρ^{MA} has a single peak at half filling. The coefficient $C_L^{\text{MA}} = C_\rho^{\text{MA}} - C_\kappa^{\text{MA}}$ for the order T^2 term of the Lorenz number $L_{\text{MA}} \equiv \kappa_{\text{MA}}/(\sigma_{\text{MA}}T)$ for magnetic alloys also becomes less sensitive to the electron filling N_d compared to C_L^{QD} for quantum dots.

The three-body correlation functions can be determined experimentally by measuring the coefficients C 's for the next leading order terms. These experimental values can then be used to infer the behaviors of other unmeasured transport coefficients.

ACKNOWLEDGMENTS

This work was supported by JSPS KAKENHI Grants No. JP18K03495, No. JP18J10205, No. JP21K03415, and No. 23K03284 and JST CREST Grant No. JPMJCR1876. K. M. was supported by JST Establishment of University Fellowships towards the Creation of Science Technology Innovation Grant No. JPMJFS2138. Y. T. was supported by Sasakawa Scientific Research Grant from the Japan Science Society No. 2021-2009, and by the Shigemasa and Shigeaki Nakazawa Fellowship of Graduate School of Science, Osaka City University.

Appendix A: Fermi liquid parameters

1. Linear and nonlinear static susceptibilities

The ground-state properties and the leading Fermi liquid corrections due to the low-lying excitations can be described in terms of the occupation number and the linear susceptibilities of the impurity level, derived from the free energy $\Omega \equiv -(1/\beta) \log [\text{Tr} e^{-\beta\mathcal{H}}]$:

$$\langle n_{d\sigma} \rangle = \frac{\partial\Omega}{\partial\epsilon_{d\sigma}}, \quad (\text{A1})$$

$$\chi_{\sigma\sigma'} \equiv -\frac{\partial^2\Omega}{\partial\epsilon_{d\sigma}\partial\epsilon_{d\sigma'}} = \int_0^\beta d\tau \langle \delta n_{d\sigma}(\tau) \delta n_{d\sigma'} \rangle. \quad (\text{A2})$$

Here, $\delta n_{d\sigma} \equiv n_{d\sigma} - \langle n_{d\sigma} \rangle$, and thermal-equilibrium averages are defined as $\langle O \rangle = \text{Tr} [e^{-\beta\mathcal{H}} O] / \text{Tr} e^{-\beta\mathcal{H}}$, with $\beta = 1/T$ the inverse temperature.

In addition to the linear susceptibilities, the nonlinear susceptibilities $\chi_{\sigma_1\sigma_2\sigma_3}^{[3]}$ play an essential role in the next-leading order terms of the transport coefficients when the system does not have both the electron-hole and time-reversal symmetries:

$$\begin{aligned} \chi_{\sigma_1\sigma_2\sigma_3}^{[3]} &\equiv -\frac{\partial^3\Omega}{\partial\epsilon_{d\sigma_1}\partial\epsilon_{d\sigma_2}\partial\epsilon_{d\sigma_3}} = \frac{\partial\chi_{\sigma_1\sigma_2}}{\partial\epsilon_{d\sigma_3}} \\ &= -\int_0^\beta d\tau_1 \int_0^\beta d\tau_2 \langle T_\tau \delta n_{d\sigma_1}(\tau_1) \delta n_{d\sigma_2}(\tau_2) \delta n_{d\sigma_3} \rangle. \end{aligned} \quad (\text{A3})$$

Here, T_τ is the imaginary-time ordering operator. This correlation function has the permutation symmetry: $\chi_{\sigma_1\sigma_2\sigma_3}^{[3]} = \chi_{\sigma_2\sigma_1\sigma_3}^{[3]} = \chi_{\sigma_3\sigma_2\sigma_1}^{[3]} = \chi_{\sigma_1\sigma_3\sigma_2}^{[3]} = \dots$. Specifically, in our formulation we are using the ground state values for $\langle n_{d\sigma} \rangle$, $\chi_{\sigma\sigma'}$ and $\chi_{\sigma_1\sigma_2\sigma_3}^{[3]}$, determined at $T = 0$.

The occupation number can be related to the phase shift δ_σ through the Friedel sum rule: $\langle n_{d\sigma} \rangle \xrightarrow{T \rightarrow 0} \delta_\sigma/\pi$.

The phase shift corresponds to the argument of the Green's function, given by $G_\sigma^r(0) = -|G_\sigma^r(0)|e^{i\delta_\sigma}$, at $\omega = T = eV = 0$ [8], and determines the value of the spectral function $\rho_{d\sigma}(\omega)$ at $\omega = 0$:

$$\rho_{d\sigma}(\omega) \equiv A_\sigma(\omega) \Big|_{T=eV=0}, \quad (\text{A4})$$

$$\rho_{d\sigma} \equiv \rho_{d\sigma}(0) = \frac{\sin^2 \delta_\sigma}{\pi \Delta}, \quad (\text{A5})$$

where $A_\sigma(\omega)$ is the nonequilibrium spectral function defined in Eq. (3.2). The derivative of $\rho_{d\sigma}(\omega)$ also contributes to the next-leading order terms and can be expressed in terms of the diagonal susceptibility $\chi_{\sigma\sigma}$, using Eq. (A11),

$$\rho'_{d\sigma} \equiv \frac{\partial \rho_{d\sigma}(\omega)}{\partial \omega} \Big|_{\omega=0} = -\frac{\partial \rho_{d\sigma}}{\partial \epsilon_{d\sigma}} = \frac{\chi_{\sigma\sigma}}{\Delta} \sin 2\delta_\sigma. \quad (\text{A6})$$

One of the most typical Fermi liquid corrections due to many-body scatterings arises in the T -linear specific heat $\mathcal{C}_{\text{imp}}^{\text{heat}}$ of impurity electrons:

$$\mathcal{C}_{\text{imp}}^{\text{heat}} = \gamma_{\text{imp}} T, \quad \gamma_{\text{imp}} \equiv \frac{\pi^2}{3} \sum_{\sigma} \chi_{\sigma\sigma}. \quad (\text{A7})$$

The coefficient γ_{imp} can be expressed in terms of the diagonal components of the linear susceptibility $\chi_{\sigma\sigma}$ using the Ward identities [6, 8, 9], i.e., Eqs. (A11) and (A12), which follow from a relationship between the derivative of the self-energy with respect to ω and the derivative with respect to $\epsilon_{d\sigma}$.

2. Ward identities

The local Fermi liquid state of quantum impurity systems can be microscopically described using the retarded Green's function, defined in Eq. (3.1), which can also be written in the form,

$$G_\sigma^r(\omega) = \frac{1}{\omega - \epsilon_{d\sigma} + i\Delta - \Sigma_\sigma^r(\omega)}. \quad (\text{A8})$$

The information about the low-lying energy states can be extracted from the equilibrium self-energy $\Sigma_{\text{eq},\sigma}^r(\omega) \equiv \Sigma_\sigma^r(\omega)|_{T=eV=0}$, by expanding it, step by step, around the Fermi energy $\omega = 0$. The expansion up to linear terms in

ω describes the renormalized resonance state of the form,

$$G_\sigma^r(\omega) \simeq \frac{z_\sigma}{\omega - \tilde{\epsilon}_{d\sigma} + i\tilde{\Delta}_\sigma}. \quad (\text{A9})$$

Here, the renormalized parameters are defined by

$$\begin{aligned} \tilde{\epsilon}_{d\sigma} &\equiv z_\sigma [\epsilon_{d\sigma} + \Sigma_{\text{eq},\sigma}^r(0)] = \tilde{\Delta}_\sigma \cot \delta_\sigma, \\ \tilde{\Delta}_\sigma &\equiv z_\sigma \Delta, \quad \frac{1}{z_\sigma} \equiv 1 - \frac{\partial \Sigma_{\text{eq},\sigma}^r(\omega)}{\partial \omega} \Big|_{\omega=0}. \end{aligned} \quad (\text{A10})$$

The wavefunction renormalization factor z_σ can be related to the derivative of $\Sigma_{\text{eq},\sigma}^r(0)$ with respect to the impurity level $\epsilon_{d\sigma'}$, using the Ward identity [6, 8, 9]:

$$\frac{1}{z_\sigma} = \tilde{\chi}_{\sigma\sigma'}, \quad \tilde{\chi}_{\sigma\sigma'} \equiv \delta_{\sigma\sigma'} + \frac{\partial \Sigma_{\text{eq},\sigma}^r(0)}{\partial \epsilon_{d\sigma'}}. \quad (\text{A11})$$

The coefficient $\tilde{\chi}_{\sigma\sigma'}$ determines the extent to which the susceptibility is enhanced at $T = 0$:

$$\chi_{\sigma\sigma'} = -\frac{\partial \langle n_{d\sigma} \rangle}{\partial \epsilon_{d\sigma'}} \xrightarrow{T \rightarrow 0} \rho_{d\sigma} \tilde{\chi}_{\sigma\sigma'}. \quad (\text{A12})$$

Recently studies have been clarified that the order ω^2 real part of the self-energy can be expressed in terms of the diagonal component of the three-body correlation function, $\chi_{\sigma\sigma\sigma}^{[3]}$, as [18–21]

$$\frac{\partial^2}{\partial \omega^2} \text{Re} \Sigma_{\text{eq},\sigma}^r(\omega) \Big|_{\omega \rightarrow 0} = \frac{\partial^2 \Sigma_{\text{eq},\sigma}^r(0)}{\partial \epsilon_{d\sigma}^2} = \frac{\partial \tilde{\chi}_{\sigma\sigma}}{\partial \epsilon_{d\sigma}}. \quad (\text{A13})$$

Physically, this coefficient determines the energy shifts of quasiparticles of order ω^2 , T^2 and $(eV)^2$, which affect the low-energy transport of the next-leading order.

Appendix B: Low-energy asymptotic form of spectral function

The low-energy asymptotic form of the retarded self-energy $\Sigma_\sigma^r(\omega)$ for multilevel Anderson impurity model has been derived up to terms of order ω^2 , T^2 , and $(eV)^2$ in the previous works [27, 29]. For symmetric tunnel junctions with $\Gamma_L = \Gamma_R (= \Delta/2)$ and $\mu_L = -\mu_R (= eV/2)$, it takes the form,

$$\text{Im} \Sigma_\sigma^r(\omega) = -\frac{\pi}{2} \frac{1}{\rho_{d\sigma}} \sum_{\sigma' (\neq \sigma)} \chi_{\sigma\sigma'}^2 \left[\omega^2 + \frac{3}{4} (eV)^2 + (\pi T)^2 \right] + \dots, \quad (\text{B1})$$

$$\epsilon_{d\sigma} + \text{Re} \Sigma_\sigma^r(\omega) = \Delta \cot \delta_\sigma + (1 - \tilde{\chi}_{\sigma\sigma}) \omega + \frac{1}{2} \frac{\partial \tilde{\chi}_{\sigma\sigma}}{\partial \epsilon_{d\sigma}} \omega^2 + \frac{1}{6} \frac{1}{\rho_{d\sigma}} \sum_{\sigma' (\neq \sigma)} \chi_{\sigma\sigma'\sigma'}^{[3]} \left[\frac{3}{4} (eV)^2 + (\pi T)^2 \right] + \dots. \quad (\text{B2})$$

Substituting these expansion results into Eq. (A8), we obtain the asymptotic form spectral function,

$$\begin{aligned} \pi \Delta A_\sigma(\omega) &= \sin^2 \delta_\sigma + \frac{\pi^2}{3} \left(\frac{3}{2} \cos 2\delta_\sigma \sum_{\sigma'(\neq\sigma)} \chi_{\sigma\sigma'}^2 - \frac{\sin 2\delta_\sigma}{2\pi} \sum_{\sigma'(\neq\sigma)} \chi_{\sigma\sigma'\sigma'}^{[3]} \right) \left[\frac{3}{4} (eV)^2 + (\pi T)^2 \right] \\ &+ \pi \sin 2\delta_\sigma \chi_{\sigma\sigma} \omega + \pi^2 \left[\cos 2\delta_\sigma \left(\chi_{\sigma\sigma}^2 + \frac{1}{2} \sum_{\sigma'(\neq\sigma)} \chi_{\sigma\sigma'}^2 \right) - \frac{\sin 2\delta_\sigma}{2\pi} \chi_{\sigma\sigma\sigma}^{[3]} \right] \omega^2 + \dots \end{aligned} \quad (\text{B3})$$

Correspondingly, the inverse of the spectral function that determines the thermoelectric transport of magnetic alloys takes the following form, up to terms order ω^2 and T^2 at $eV = 0$,

$$\begin{aligned} \frac{1}{\pi \Delta A_\sigma(\omega)} &\simeq \frac{1}{\pi \Delta \rho_{d\sigma}} \left[1 - \frac{1}{6 \Delta \rho_{d\sigma}} \left(3\pi \cos 2\delta_\sigma \sum_{\sigma'(\neq\sigma)} \chi_{\sigma\sigma'}^2 - \sin 2\delta_\sigma \sum_{\sigma'(\neq\sigma)} \chi_{\sigma\sigma'\sigma'}^{[3]} \right) (\pi T)^2 - \frac{\sin 2\delta_\sigma \chi_{\sigma\sigma\sigma}^{[3]}}{\Delta \rho_{d\sigma}} \omega \right. \\ &\left. + \frac{\pi}{\Delta \rho_{d\sigma}} \left\{ (\cos 2\delta_\sigma + 2) \chi_{\sigma\sigma}^2 - \frac{1}{2} \cos 2\delta_\sigma \sum_{\sigma'(\neq\sigma)} \chi_{\sigma\sigma'}^2 + \frac{\sin 2\delta_\sigma}{2\pi} \chi_{\sigma\sigma\sigma}^{[3]} \right\} \omega^2 \right] + \dots \end{aligned} \quad (\text{B4})$$

Appendix C: Properties of $\chi_{\sigma_1\sigma_2\sigma_3}^{[3]}$ in SU(N) case

We briefly describe here some relations between the three-body correlation functions and the derivative of the linear susceptibilities with respect to the center of mass coordinate of the impurity levels, $\epsilon_d \equiv (1/N) \sum_\sigma \epsilon_{d\sigma}$.

The derivative of the diagonal susceptibility $\chi_{\sigma\sigma}$ can be written as

$$\begin{aligned} \frac{\partial \chi_{\sigma\sigma}}{\partial \epsilon_d} &= \frac{\partial \chi_{\sigma\sigma}}{\partial \epsilon_{d\sigma}} + \sum_{\sigma'(\neq\sigma)} \frac{\partial \chi_{\sigma\sigma}}{\partial \epsilon_{d\sigma'}} \\ &\xrightarrow{\text{SU}(N)} \chi_{\sigma\sigma\sigma}^{[3]} + (N-1) \chi_{\sigma\sigma'\sigma'}^{[3]}, \end{aligned} \quad (\text{C1})$$

where $\sigma \neq \sigma'$. Note that $\chi_{\sigma\sigma\sigma}^{[3]} = \chi_{\sigma\sigma'\sigma'}^{[3]}$ in the SU(N) symmetric case. Similarly, the derivative of the off-diagonal susceptibility $\chi_{\sigma\sigma'}$ for $\sigma \neq \sigma'$ takes the form

$$\begin{aligned} \frac{\partial \chi_{\sigma\sigma'}}{\partial \epsilon_d} &= \frac{\partial \chi_{\sigma\sigma'}}{\partial \epsilon_{d\sigma}} + \frac{\partial \chi_{\sigma\sigma'}}{\partial \epsilon_{d\sigma'}} + \sum_{\substack{\sigma''(\neq\sigma \\ \neq\sigma')}} \frac{\partial \chi_{\sigma\sigma'}}{\partial \epsilon_{d\sigma''}} \\ &\xrightarrow{\text{SU}(N)} 2 \chi_{\sigma\sigma'\sigma'}^{[3]} + (N-2) \chi_{\sigma\sigma'\sigma''}^{[3]}, \end{aligned} \quad (\text{C2})$$

for $\sigma \neq \sigma' \neq \sigma'' \neq \sigma$. In the SU(2) symmetric case, Eqs. (C1) and (C2) provide enough information to determine the two independent components $\chi_{\sigma\sigma\sigma}^{[3]}$ and $\chi_{\sigma\sigma'\sigma'}^{[3]}$ from the two differential coefficients $\partial \chi_{\sigma\sigma} / \partial \epsilon_d$ and $\partial \chi_{\sigma\sigma'} / \partial \epsilon_d$. However, for $N \geq 3$, there are three independent three-body components, i.e., $\chi_{\sigma\sigma\sigma}^{[3]}$, $\chi_{\sigma\sigma'\sigma'}^{[3]}$, and $\chi_{\sigma\sigma'\sigma''}^{[3]}$, so that we need additional information to determine all these components.

In order to obtain another independent relation, we consider the derivative of the susceptibilities with respect to the magnetic field b , which induces the level splitting in impurity levels $\epsilon_{d\sigma}$ in a such way that $\epsilon_{d,m,\uparrow} = \epsilon_d - b$

and $\epsilon_{d,m,\downarrow} = \epsilon_d + b$, with $\sigma = (m, s)$ for $m = 1, 2, \dots, N/2$ and $s = \uparrow, \downarrow$:

$$\begin{aligned} \frac{\partial \chi_{m_1 s_1, m_2 s_2}}{\partial b} &= \sum_{m_3=1}^{N/2} \sum_{s_3=\uparrow, \downarrow} \frac{\partial \epsilon_{d, m_3, s_3}}{\partial b} \frac{\partial \chi_{m_1 s_1, m_2 s_2}}{\partial \epsilon_{d, m_3, s_3}} \\ &= - \sum_{m_3=1}^{N/2} \chi_{m_1 s_1, m_2 s_2, m_3 \uparrow}^{[3]} + \sum_{m_3=1}^{N/2} \chi_{m_1 s_1, m_2 s_2, m_3 \downarrow}^{[3]}. \end{aligned} \quad (\text{C3})$$

From this derivative, we obtain the following relation, taking $m_1 = m_2 (\equiv m)$,

$$\begin{aligned} \frac{\partial}{\partial b} \left(\frac{\chi_{m\uparrow, m\uparrow} - \chi_{m\downarrow, m\downarrow}}{2} \right) &= - \sum_{m'=1}^{N/2} \frac{1}{2} \left(\chi_{m\uparrow, m\uparrow, m'\uparrow}^{[3]} - \chi_{m\uparrow, m\uparrow, m'\downarrow}^{[3]} \right. \\ &\quad \left. + \chi_{m\downarrow, m\downarrow, m'\downarrow}^{[3]} - \chi_{m\downarrow, m\downarrow, m'\uparrow}^{[3]} \right) \\ &\xrightarrow{b \rightarrow 0} - \sum_{m_3=1}^{N/2} \left[\chi_{m\uparrow, m\uparrow, m_3 \uparrow}^{[3]} - \chi_{m\uparrow, m\uparrow, m_3 \downarrow}^{[3]} \right] \\ &= - \left(\chi_{m\uparrow, m\uparrow, m\uparrow}^{[3]} - \chi_{m\uparrow, m\uparrow, m\downarrow}^{[3]} \right). \end{aligned} \quad (\text{C4})$$

Here, we set the magnetic field to be zero, $b = 0$, in the last two lines. This relation can also be rewritten into the following form at $b = 0$, using the original label $\sigma = (m, s)$,

$$\chi_B^{[3]} \equiv \frac{\partial}{\partial b} \left(\frac{\chi_{m\uparrow, m\uparrow} - \chi_{m\downarrow, m\downarrow}}{2} \right)_{b=0} = -\chi_{\sigma\sigma\sigma}^{[3]} + \chi_{\sigma\sigma'\sigma'}^{[3]}, \quad (\text{C5})$$

for $\sigma' \neq \sigma$.

Appendix D: NRG procedures

We have carried out NRG calculations, dividing the N conduction channels into $N/2$ pairs and using the SU(2) spin and U(1) charge symmetries for each of the pairs, i.e., $\prod_{k=1}^{N/2} \{SU(2) \otimes U(1)\}_k$ symmetries. The discretization parameter Λ and the number of retained low-lying excited states N_{trunc} are chosen to be $(\Lambda, N_{\text{trunc}}) = (6, 10000)$ for $N = 4$. Note that the SU(4) symmetry is preserved in our iteration scheme since the truncation of higher energy states has been carried out after adding all new states from the $N/2$ pairs.

For $N = 6$, we have also exploited the method of Stadler *et al.* [85]. In this case, the truncation procedure is carried out at each of the steps ($k=1, 2, \dots, N/2$) after adding the states constructed with one of the channel pairs, by using Oliveira's \mathcal{Z} -trick [86], choosing different \mathcal{Z} values for each of the $N/2$ steps: $\mathcal{Z}_k = 1/2 + k/N$ for the k -th pair. We have carried out calculations for $N = 6$, taking rather large values for the NRG parameters, such that $(\Lambda, N_{\text{trunc}}) = (20, 40000)$ for small interactions $U/(\pi\Delta) = 2/5$ and 1, and $(20, 30000)$ for large interactions $U/(\pi\Delta) = 2, 3, 4, 5$, and 6. This method significantly reduces the computational cost for obtaining low-lying energy states and enables us to calculate the three-body correlation functions for 6, although it does not faithfully preserve the SU(6) symmetry. We have checked whether this method reproduces the non-interacting results. Figure 14 compares the NRG result for $\sin^2 \delta$ with the exact one for $U = 0$; the results show reasonable agreement. It indicates that this truncation procedure works effectively for deducing the SU(6) FL parameters.

In order to calculate $\chi_B^{[3]}$ defined in Eq. (5.13), we have also introduced a small external potential $\epsilon_{\text{sp},k}$, which depends on the channel index $k=1, 2, \dots, N/2$ and shifts the impurity level from ϵ_d . Specifically, for $N = 4$, it is applied in a way equivalent to the local Zeeman field: $\epsilon_{\text{sp},1} = -b$ and $\epsilon_{\text{sp},2} = b$. For $N = 6$, we have

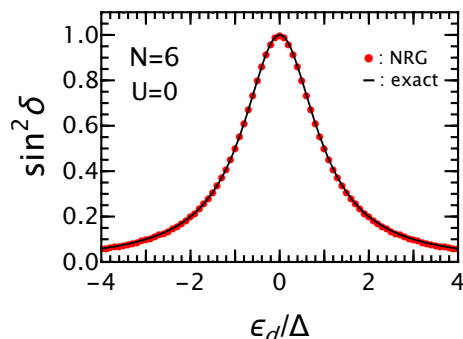


FIG. 14. Comparison of (•) NRG and (—) exact results of $\sin^2 \delta$ for $U = 0$. The NRG calculation was performed for $N = 6$, taking $\Lambda = 20$ and keeping $N_{\text{trunc}} = 40000$ low-energy states.

extended the potential such that $\epsilon_{\text{sp},1} = -b$, $\epsilon_{\text{sp},2} = 0$, and $\epsilon_{\text{sp},3} = b$, and have deduced $\chi_B^{[3]}$ from the derivatives of the channel susceptibilities with respect to b .

Appendix E: Two-body FL parameters for SU(4) & SU(6) symmetric cases

We provide a quick overview of the behavior of the renormalized parameters in the SU(4) and SU(6) cases, which can be derived from the phase shift and the linear susceptibilities [87–90]. Our discussion here is based on the NRG results, plotted in Figs. 15 and 16 as functions of the impurity level position ξ_d , for several different interaction strengths: from weak to strong interactions up to $U/(\pi\Delta) = 6.0$.

The SU(N) Kondo effect occurs for strong interactions when the impurity levels are filled by an integer number of electrons, i.e., at the fillings of $N_d = 1, 2, \dots, N - 1$. It takes place at $\xi_d \simeq 0, \pm U, \dots, \pm \frac{N-2}{2}U$, and gives an interesting variety in the low-energy properties. As N increases, a greater interaction strength is required to clearly observe the Kondo behavior. This is because the quantum fluctuations caused by the Coulomb interaction are suppressed for large N . In particular, the mean-field theory becomes exact in the limit $N \rightarrow \infty$ that is taken keeping the scaled interaction $U^* \equiv (N - 1)U$ constant [90].

Figures 15(a) and 16(a) show the occupation number N_d for $N = 4$ and 6, respectively. As U increases, the Coulomb staircase structure emerges: N_d varies steeply at $\xi_d \simeq \pm U/2, \pm 3U/2, \dots, \pm (N - 1)U/2$. Correspondingly, as U increases, the transmission probability $\sin^2 \delta$, shown in Figs. 15(b) and 16(b), exhibits a plateau structure that develops around $\xi_d \simeq 0, \pm U, \dots, \pm (N - 2)U/2$. In particular, the plateau at the half-filling point $\xi_d \simeq 0$ reaches the unitary limit value $\sin^2 \delta = 1.0$.

The renormalization factor z , shown in Figs. 15(c) and 16(c) for $N = 4$ and 6, exhibits a broad valley structure at $|\xi_d| \lesssim (N - 1)U/2$, where $1 \lesssim N_d \lesssim N - 1$. The valley becomes deeper as U increases, and the local minima emerge for $U/(\pi\Delta) \gtrsim 3.0$ at the integer-filling points, reflecting the occurrence of the SU(N) Kondo effects. The renormalization factor also has local maxima at intermediate valence states in between two adjacent local minima. Note that z is significantly suppressed by the strong electron correlations even at these local maxima. Figures 15(d) and 16(d) show the rescaled Wilson ratio $\tilde{K} \equiv (N - 1)(R - 1)$. For large interactions, \tilde{K} exhibits a wide flat structure at $|\xi_d| \lesssim (N - 1)U/2$, the height of which approaches the saturation value $\tilde{K} \simeq 1.0$, especially for $U/(\pi\Delta) \gtrsim 3.0$, reflecting the suppression of charge fluctuations in this region of ξ_d .

Figures 15(e) and 16(e) show the renormalized resonance-level position $\tilde{\epsilon}_d \equiv z\Delta \cot \delta$ for $N = 4$ and 6, respectively, as a function of ξ_d . For strong interactions, the renormalized level is almost locked at the

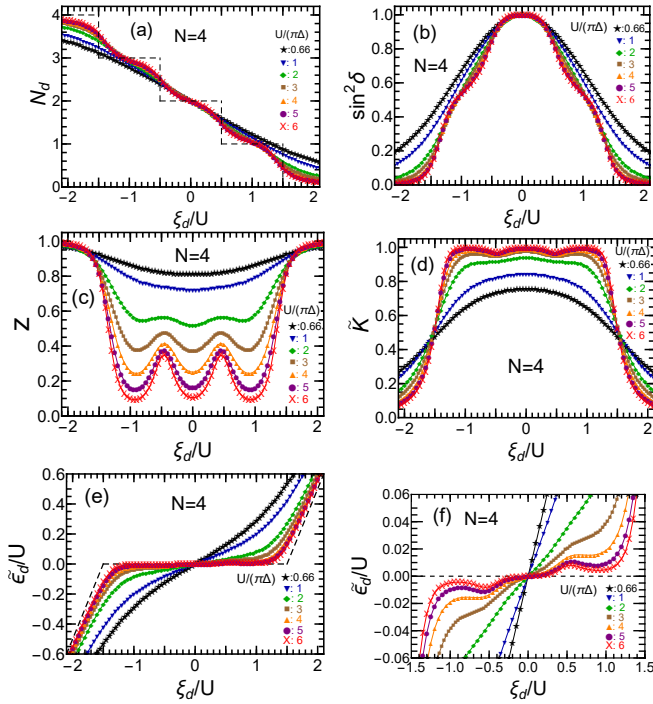


FIG. 15. Fermi liquid parameters for the SU(4) symmetric Anderson model are plotted vs ξ_d : (a) N_d , (b) $\sin^2 \delta$, (c) renormalization factor z , (d) $\tilde{K} = (N-1)(R-1)$. (e) renormalized level $\tilde{\epsilon}_d$, and (f) enlarged view of $\tilde{\epsilon}_d$. Interaction strengths are chosen to be $U/(\pi\Delta) = 2/3(\star)$, $1(\blacktriangledown)$, $2(\blacklozenge)$, $3(\blacksquare)$, $4(\blacktriangle)$, $5(\bullet)$, $6(\times)$. The dashed line in (a) represents N_d in the atomic limit $\Delta \rightarrow 0$.

Fermi level, $\tilde{\epsilon}_d \simeq 0.0$, in the strong-coupling region $|\xi_d| \lesssim (N-1)U/2$, which corresponds to the filling range of $1 \lesssim N_d \lesssim N-1$. Figures 15(f) and 16(f) show an enlarged view of $\tilde{\epsilon}_d$ in the vicinity of the Fermi level. We see that $\tilde{\epsilon}_d$ exhibits a fine structure which reflects the staircase behavior of the phase shift δ and the oscillatory behavior of the renormalization factor z . Outside the strong-coupling region, $\tilde{\epsilon}_d$ approaches the bare value $\tilde{\epsilon}_d \simeq \epsilon_d$ at $\xi_d \gg (N-1)U/2$, or the Hartree-Fock value $\tilde{\epsilon}_d \simeq \epsilon_d + (N-1)U$ at $\xi_d \ll -(N-1)U/2$: these asymptotic forms of $\tilde{\epsilon}_d$ are shown as the dashed lines in Figs. 15(e) and 16(e).

Appendix F: Current noise and thermoelectric transport for SU(2) symmetric case

We have discussed the behavior of the current noise and thermoelectric transport of the SU(4) and SU(6) Anderson model in Secs. VII, VIII, and X. For comparison, here we briefly describe the corresponding results in the SU(2) case, specifically, the current noise and the thermoelectric transport coefficients are plotted in Figs. 17 and 18, respectively.

We can see in Fig. 17(b) that the linear noise is suppressed in the strong-coupling region $|\xi_d| \lesssim U/2$ for large

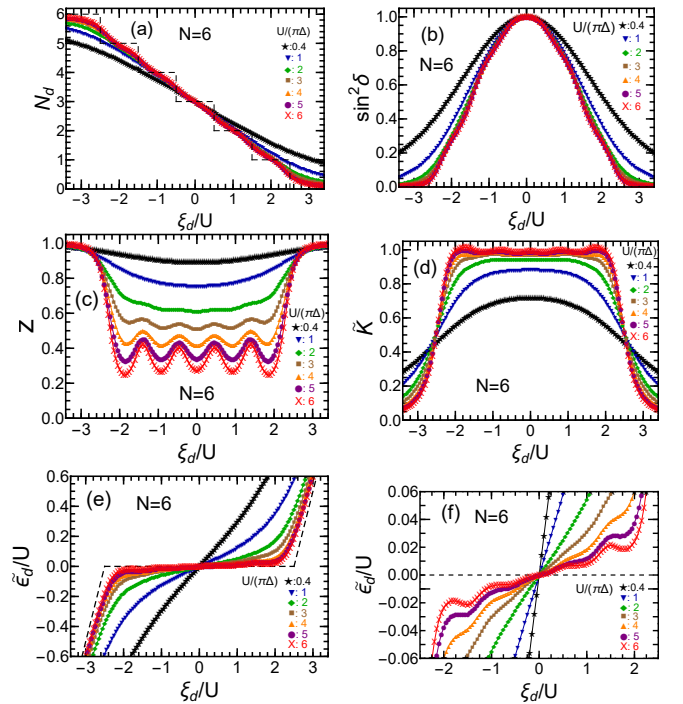


FIG. 16. Fermi liquid parameters for the SU(6) symmetric Anderson model are plotted vs ξ_d : (a) N_d , (b) $\sin^2 \delta$, (c) renormalization factor z , (d) $\tilde{K} = (N-1)(R-1)$. (e) renormalized level $\tilde{\epsilon}_d$, and (f) enlarged view of $\tilde{\epsilon}_d$. Interaction strengths are chosen to be $U/(\pi\Delta) = 2/5(\star)$, $1(\blacktriangledown)$, $2(\blacklozenge)$, $3(\blacksquare)$, $4(\blacktriangle)$, $5(\bullet)$, $6(\times)$. The dashed line in (a) represents N_d in the atomic limit $\Delta \rightarrow 0$.

U , where the transmission probability exhibits a wide Kondo plateau in Fig. 17(a). However, the linear noise increases and has the peaks, the width of which is of the order of Δ at valence fluctuation regions near the quarter and three-quarters filling points where the phase reaches $\delta = \pi/4$ or $3\pi/4$. At these filling points, the coefficient C_S for the order $|eV|^3$ nonlinear current noise has the negative minima, as seen in Fig. 17(c). We see in Fig. 17(d) that the three-body part Θ_S of C_S , is also suppressed over a wide region $|\xi_d| \lesssim U/2$. Therefore, in this strong-coupling region, the nonlinear noise C_S is determined solely by the two-body part W_S in the SU(2) case:

$$W_S = 4(R-1)^2 + \left[1 + 5(R-1)^2\right] \cos 4\delta, \quad (\text{F1})$$

where R is the Wilson ratio. In particular, the dip structures of C_S at the quarter and three-quarters fillings reflect the minima of $\cos 4\delta$ in W_S . In contrast, at $|\xi_d| \gtrsim U/2$, the three-body part Θ_S becomes comparable to W_S , and contributes to C_S .

Figure 18 shows the results for the next-leading order terms of the thermoelectric transport coefficients for the SU(2) quantum dots (a) C_T and (b) C_κ^{QD} , and for SU(2) magnetic alloys (c) C_ρ^{MA} and (d) C_κ^{MA} . All these coefficients exhibit the plateau structures due to the Kondo effect in the strong-coupling region $|\xi_d| \lesssim U/2$ for large

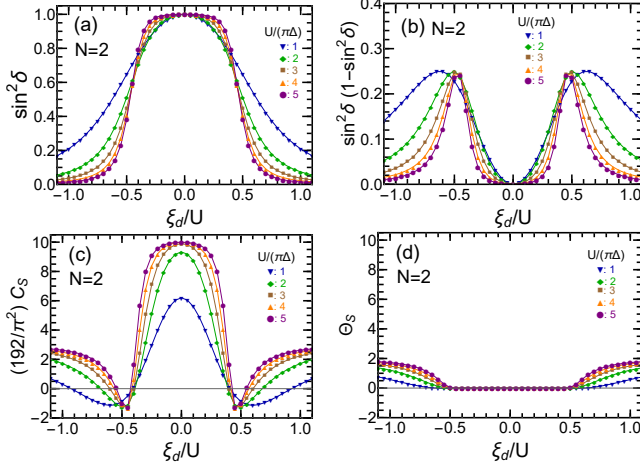


FIG. 17. Current noise for SU(2) symmetric quantum dots vs ξ_d : (a) $\sin^2 \delta$, (b) linear noise $\sin^2 \delta (1 - \sin^2 \delta)$, (c) $(192/\pi^2) C_S = W_S + \Theta_S$, (d) $\Theta_S = -(\Theta_I + 3\tilde{\Theta}_{II}) \cos 2\delta$ (see Table II). Interaction strengths are chosen to be $U/(\pi\Delta) = 1(\blacktriangledown), 2(\blacklozenge), 3(\blacksquare), 4(\blacktriangle), 5(\bullet)$.

U , where the phase shift is locked at $\delta \simeq \pi/2$. In this region, the three-body contributions, Θ_I and $\tilde{\Theta}_{II}$, almost vanish (see Ref. 28 for more details), and the height of these plateaus approach the saturation values for $U \rightarrow \infty$, i.e., $(48/\pi^2)C_T \rightarrow 3$, $(48/\pi^2)C_\rho^{\text{MA}} \rightarrow 3$, $[80/(7\pi^2)]C_\kappa^{\text{QD}} \rightarrow 13/7$, and $[80/(7\pi^2)]C_\kappa^{\text{MA}} \rightarrow 13/7$. The coefficients C_T and C_ρ^{MA} for charge transport show a similar behavior in the strong-coupling region. Furthermore, in this region, the coefficients for thermal conductivities, C_κ^{QD} and C_κ^{MA} , also show a similar behavior. In contrast, at $|\xi_d| \gtrsim U/2$, the coefficients C_T and C_κ^{QD} for quantum dots change sign and become negative as the occupation number approaches $N_d \simeq 0.0$ or 2.0 , whereas the coefficients C_ρ^{MA} and C_κ^{MA} for magnetic alloys remain positive definite.

Appendix G: Three-body Fermi liquid corrections to thermoelectric transport of magnetic alloys

In this appendix, we describe the low-energy asymptotic form of the electrical resistivity $\varrho_{\text{MA}} = 1/\sigma_{\text{MA}}$, the thermopower \mathcal{S}_{MA} , and the thermal conductivity κ_{MA} of magnetic alloys:

$$\sigma_{\text{MA}} = \sigma_{\text{MA}}^{\text{unit}} \frac{1}{N} \sum_{\sigma} \mathcal{L}_{0,\sigma}^{\text{MA}}, \quad (\text{G1})$$

$$\mathcal{S}_{\text{MA}} = \frac{-1}{|e|T} \frac{\sum_{\sigma} \mathcal{L}_{1,\sigma}^{\text{MA}}}{\sum_{\sigma} \mathcal{L}_{0,\sigma}^{\text{MA}}}, \quad (\text{G2})$$

$$\kappa_{\text{MA}} = \frac{\sigma_{\text{MA}}^{\text{unit}}}{e^2 T} \frac{1}{N} \left[\sum_{\sigma} \mathcal{L}_{2,\sigma}^{\text{MA}} - \frac{(\sum_{\sigma} \mathcal{L}_{1,\sigma}^{\text{MA}})^2}{\sum_{\sigma} \mathcal{L}_{0,\sigma}^{\text{MA}}} \right]. \quad (\text{G3})$$

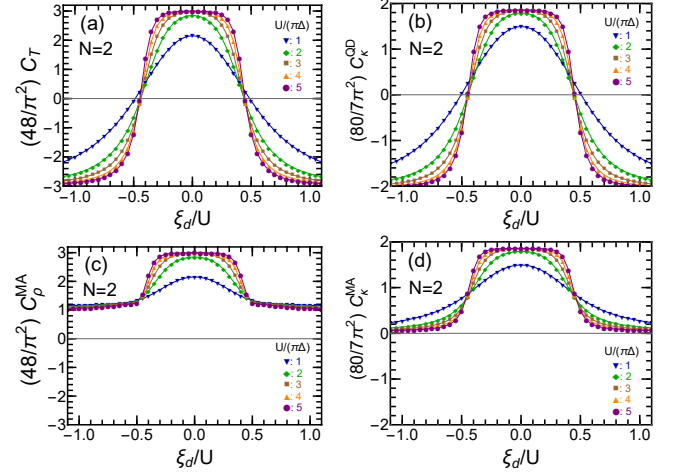


FIG. 18. Next-leading order terms of transport coefficients for an SU(2) symmetric Anderson impurity: (a) $(48/\pi^2)C_T$, (b) $[80/(7\pi^2)]C_\kappa^{\text{QD}}$, (c) $(48/\pi^2)C_\rho^{\text{MA}}$, and (d) $[80/(7\pi^2)]C_\kappa^{\text{MA}}$, defined in Table II. Interaction strengths are chosen to be $U/(\pi\Delta) = 1(\blacktriangledown), 2(\blacklozenge), 3(\blacksquare), 4(\blacktriangle), 5(\bullet)$.

For magnetic alloys, the response functions $\mathcal{L}_{n,\sigma}^{\text{MA}}$ for $n = 0, 1$ and 2 are given by

$$\mathcal{L}_{n,\sigma}^{\text{MA}} = \int_{-\infty}^{\infty} d\omega \frac{\omega^n}{\pi \Delta A_\sigma(\omega)} \left(-\frac{\partial f(\omega)}{\partial \omega} \right). \quad (\text{G4})$$

Equation (G1) defines the electrical conductivity relative to its unitary-limit value $\sigma_{\text{MA}}^{\text{unit}}$. Correspondingly, the prefactor for κ_{MA} is defined in such a way that the T -linear thermal conductivity should take the form,

$$\lim_{T \rightarrow 0} \frac{\kappa_{\text{MA}}}{T} = \frac{\pi^2}{3e^2} \sigma_{\text{MA}}^{\text{unit}}. \quad (\text{G5})$$

The asymptotic form of $\mathcal{L}_{n,\sigma}^{\text{MA}}$ can be calculated, using the low-energy expansion of the inverse spectral function $1/A_\sigma(\omega)$ given in Eq. (B4):

$$\mathcal{L}_{0,\sigma}^{\text{MA}} = \frac{1}{\sin^2 \delta_\sigma} \left[1 + \frac{a_{0,\sigma}^{\text{MA}}}{\sin^2 \delta_\sigma} (\pi T)^2 \right] + \dots, \quad (\text{G6})$$

$$\mathcal{L}_{1,\sigma}^{\text{MA}} = -\frac{1}{3} \frac{\rho'_{d\sigma}}{\pi \Delta \rho_{d\sigma}^2} (\pi T)^2 + \dots, \quad (\text{G7})$$

$$\mathcal{L}_{2,\sigma}^{\text{MA}} = \frac{(\pi T)^2}{3 \sin^2 \delta_\sigma} \left[1 + \frac{a_{2,\sigma}^{\text{MA}}}{\sin^2 \delta_\sigma} (\pi T)^2 \right] + \dots. \quad (\text{G8})$$

Here, the coefficients $a_{0,\sigma}^{\text{MA}}$ and $a_{2,\sigma}^{\text{MA}}$ are given by

$$a_{0,\sigma}^{\text{MA}} = \frac{\pi^2}{3} \left[(\cos 2\delta_\sigma + 2) \chi_{\sigma\sigma}^2 - 2 \cos 2\delta_\sigma \sum_{\sigma'(\neq\sigma)} \chi_{\sigma\sigma'}^2 + \frac{\sin 2\delta_\sigma}{2\pi} \left(\chi_{\sigma\sigma\sigma}^{[3]} + \sum_{\sigma'(\neq\sigma)} \chi_{\sigma\sigma'\sigma'}^{[3]} \right) \right], \quad (\text{G9})$$

$$a_{2,\sigma}^{\text{MA}} = \frac{7\pi^2}{5} \left[(\cos 2\delta_\sigma + 2) \chi_{\sigma\sigma}^2 - \frac{6}{7} \cos 2\delta_\sigma \sum_{\sigma'(\neq\sigma)} \chi_{\sigma\sigma'}^2 + \frac{\sin 2\delta_\sigma}{2\pi} \left(\chi_{\sigma\sigma\sigma}^{[3]} + \frac{5}{21} \sum_{\sigma'(\neq\sigma)} \chi_{\sigma\sigma'\sigma'}^{[3]} \right) \right]. \quad (\text{G10})$$

We obtain the low-temperature expressions of $\varrho_{\text{MA}} = 1/\sigma_{\text{MA}}$, \mathcal{S}_{MA} and $1/\kappa_{\text{MA}}$, substituting Eqs. (G6)–(G8) into Eqs. (G1)–(G3):

$$\varrho_{\text{MA}} = \frac{1}{\sigma_{\text{MA}}^{\text{unit}}} \left[(\overline{\sin^2 \delta})_{\text{HM}} - c_\rho^{\text{MA}} (\pi T)^2 + \dots \right], \quad (\text{G11})$$

$$\mathcal{S}_{\text{MA}} = \frac{\pi^2}{3} \frac{\sum_\sigma \rho'_{d\sigma}}{\sum_\sigma \rho_{d\sigma}} \frac{T}{|e|} + \dots, \quad (\text{G12})$$

$$\frac{1}{\kappa_{\text{MA}}} = \frac{3e^2}{\pi^2 \sigma_{\text{MA}}^{\text{unit}}} \frac{1}{T} \left[(\overline{\sin^2 \delta})_{\text{HM}} - c_\kappa^{\text{MA}} (\pi T)^2 + \dots \right]. \quad (\text{G13})$$

Here, $(\overline{\sin^2 \delta})_{\text{HM}}$ is the harmonic mean (HM) of $\sin^2 \delta_\sigma$, defined by

$$(\overline{\sin^2 \delta})_{\text{HM}} \equiv \frac{1}{\frac{1}{N} \sum_\sigma \frac{1}{\sin^2 \delta_\sigma}}. \quad (\text{G14})$$

The coefficients c_ρ^{MA} and c_κ^{MA} of the next-leading order terms are given by

$$c_\rho^{\text{MA}} = \left\{ (\overline{\sin^2 \delta})_{\text{HM}} \right\}^2 \frac{1}{N} \sum_\sigma \frac{a_{0,\sigma}^{\text{MA}}}{\sin^4 \delta_\sigma}, \quad (\text{G15})$$

$$c_\kappa^{\text{MA}} = \left\{ (\overline{\sin^2 \delta})_{\text{HM}} \right\}^2 \left[\frac{1}{N} \sum_\sigma \frac{a_{2,\sigma}^{\text{MA}}}{\sin^4 \delta_\sigma} - \frac{\pi^2}{3} (\overline{\sin^2 \delta})_{\text{HM}} \left\{ \frac{1}{N} \sum_\sigma \frac{\sin 2\delta_\sigma}{\sin^4 \delta_\sigma} \chi_{\sigma\sigma} \right\}^2 \right]. \quad (\text{G16})$$

Correspondingly, the electrical conductivity and the

thermal conductivity take the following form,

$$\sigma_{\text{MA}} = \frac{\sigma_{\text{MA}}^{\text{unit}}}{(\overline{\sin^2 \delta})_{\text{HM}}} \left[1 + \frac{c_\rho^{\text{MA}}}{(\overline{\sin^2 \delta})_{\text{HM}}} (\pi T)^2 + \dots \right], \quad (\text{G17})$$

$$\kappa_{\text{MA}} = \frac{\pi^2 \sigma_{\text{MA}}^{\text{unit}} T}{3e^2 (\overline{\sin^2 \delta})_{\text{HM}}} \times \left[1 + \frac{c_\kappa^{\text{MA}}}{(\overline{\sin^2 \delta})_{\text{HM}}} (\pi T)^2 + \dots \right]. \quad (\text{G18})$$

Furthermore, the Lorenz number $L_{\text{MA}} \equiv \kappa_{\text{MA}}/(\sigma_{\text{MA}} T)$ can also be deduced up to terms of order T^2 , as

$$L_{\text{MA}} = \frac{\pi^2}{3e^2} \left[1 - \frac{c_L^{\text{MA}}}{(\overline{\sin^2 \delta})_{\text{HM}}} (\pi T)^2 + \dots \right], \quad (\text{G19})$$

$$c_L^{\text{MA}} = c_\rho^{\text{MA}} - c_\kappa^{\text{MA}}. \quad (\text{G20})$$

In the limit of zero temperature, the Lorenz number takes a constant value $L_{\text{MA}} \xrightarrow{T \rightarrow 0} \frac{\pi^2}{3e^2}$, and the Wiedemann-Franz law holds. However, it deviates as temperature increases, showing the T^2 dependence.

Appendix H: Thermoelectric transport coefficients for noninteracting magnetic alloys

We provide here the noninteracting results for the thermoelectric transport coefficients of magnetic alloys. For $U = 0$, the response functions $\mathcal{L}_{n,\sigma}^{\text{MA}}$ for $n = 0, 1, 2$ can be calculated, substituting the explicit form of the spectral function $\pi A_\sigma(\omega) \xrightarrow{U=0} \Delta/[(\omega - \epsilon_{d\sigma})^2 + \Delta^2]$ into Eq. (G4):

$$\mathcal{L}_{0,\sigma}^{\text{MA}} \xrightarrow{U=0} \left[1 + \left(\frac{\epsilon_{d\sigma}}{\Delta} \right)^2 \right] + \frac{1}{3} \left(\frac{\pi T}{\Delta} \right)^2, \quad (\text{H1})$$

$$\mathcal{L}_{1,\sigma}^{\text{MA}} \xrightarrow{U=0} \frac{-2\epsilon_{d\sigma}}{3} \left(\frac{\pi T}{\Delta} \right)^2, \quad (\text{H2})$$

$$\mathcal{L}_{2,\sigma}^{\text{MA}} \xrightarrow{U=0} \frac{\Delta^2}{3} \left[1 + \left(\frac{\epsilon_{d\sigma}}{\Delta} \right)^2 \right] \left(\frac{\pi T}{\Delta} \right)^2 + \frac{7\Delta^2}{15} \left(\frac{\pi T}{\Delta} \right)^4. \quad (\text{H3})$$

The transport coefficients, defined in Eqs. (G1)–(G3), can be deduced from these analytic expressions for $\mathcal{L}_{n,\sigma}^{\text{MA}}$. In particular, in the $\text{SU}(N)$ symmetric case where $\epsilon_{d\sigma} \equiv \epsilon_d$, the electrical resistivity $\varrho_{\text{MA}}^{(0)}$ for $U = 0$ is given by

$$\varrho_{\text{MA}}^{(0)} = \frac{1}{\sigma_{\text{MA}}^{\text{unit}}} \left[\sin^2 \delta_0 - C_\rho^{\text{MA}(0)} \left(\frac{\pi T}{T_0^*} \right)^2 \right], \quad (\text{H4})$$

$$\sin^2 \delta_0 = \frac{1}{1 + (\epsilon_d/\Delta)^2}, \quad C_\rho^{\text{MA}(0)} = \frac{\pi^2}{48}. \quad (\text{H5})$$

Here, $T_0^* \equiv \pi\Delta/(4\sin^2 \delta_0)$ is the characteristic energy scale in the noninteracting case. The coefficient $C_\rho^{\text{MA}(0)}$

for the T^2 -resistivity is given by a constant $\pi^2/48$ ($= 0.205\dots$) as the ϵ_d dependence is absorbed into T_0^* .

The thermopower S_{MA}^0 and thermal resistivity $1/\kappa_{\text{MA}}^{(0)}$ for $U = 0$ are given by

$$S_{\text{MA}}^{(0)} = \frac{1}{|e|} \frac{2\pi^2}{3} \frac{\epsilon_d}{\epsilon_d^2 + \Delta^2} T, \quad (\text{H6})$$

$$\frac{1}{\kappa_{\text{MA}}^{(0)}} = \frac{3e^2}{\pi^2 \sigma_{\text{MA}}^{\text{unit}}} \frac{1}{T} \left[\sin^2 \delta_0 - C_{\kappa}^{\text{MA}(0)} \left(\frac{\pi T}{T_0^*} \right)^2 \right], \quad (\text{H7})$$

$$C_{\kappa}^{\text{MA}(0)} = \frac{7\pi^2}{80} \frac{1 + 20 \sin^2 \delta_0}{21}. \quad (\text{H8})$$

Furthermore, the dimensionless coefficient for the order T^2 term of the Lorenz number L_{MA} is given by $C_L^{\text{MA}(0)} \equiv C_e^{\text{MA}(0)} - C_{\kappa}^{\text{MA}(0)}$ and it takes the form,

$$C_L^{\text{MA}(0)} = \frac{\pi^2}{60} (1 - 5 \sin^2 \delta_0). \quad (\text{H9})$$

These results for the next-leading order terms in the noninteracting case are plotted as functions of ϵ_d in Fig. 19. The coefficient $C_{\kappa}^{\text{MA}(0)}$ takes a Lorentzian form with an offset value of $C_{\kappa}^{\text{MA}(0)} \xrightarrow{|\epsilon_d| \rightarrow \infty} \pi^2/240$ ($= 0.041\dots$).

Correspondingly, $C_L^{\text{MA}(0)}$ has a dip at $\epsilon_d = 0$, and vanishes at the points $\epsilon_d = \pm 2\Delta$ where $C_{\kappa}^{\text{MA}(0)}$ and $C_e^{\text{MA}(0)}$ give equal contributions to the Lorenz number L_{MA} . As the impurity level moves further away from the Fermi level $|\epsilon_d| \gg \Delta$, it approaches the value of $C_L^{\text{MA}(0)} \xrightarrow{|\epsilon_d| \rightarrow \infty} \pi^2/60$ ($= 0.164\dots$).

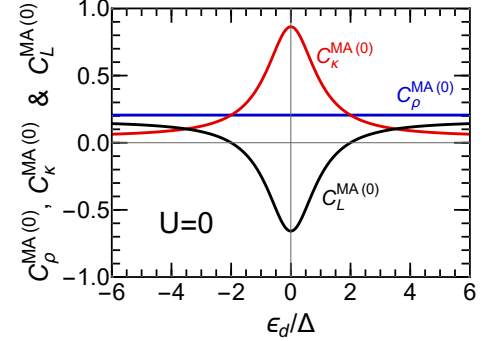


FIG. 19. Coefficients $C_e^{\text{MA}(0)}$, $C_{\kappa}^{\text{MA}(0)}$, and $C_L^{\text{MA}(0)}$ for noninteracting $U = 0$ magnetic alloys plotted vs ϵ_d .

-
- [1] J. Kondo, Prog. Theor. Phys. **32**, 37 (1964).
[2] A. C. Hewson, *The Kondo Problem to Heavy Fermions* (Cambridge University Press, Cambridge, 1993).
[3] K. Ono, J. Kobayashi, Y. Amano, K. Sato, and Y. Takahashi, Phys. Rev. A **99**, 032707 (2019).
[4] S. Yasui and S. Ozaki, Phys. Rev. D **96**, 114027 (2017).
[5] P. Nozières, J. Low Temp. Phys. **17**, 31 (1974).
[6] K. Yamada, Prog. Theor. Phys. **53**, 970 (1975).
[7] K. Yamada, Prog. Theor. Phys. **54**, 316 (1975).
[8] H. Shiba, Prog. Theor. Phys. **54**, 967 (1975).
[9] A. Yoshimori, Prog. Theor. Phys. **55**, 67 (1976).
[10] K. G. Wilson, Rev. Mod. Phys. **47**, 773 (1975).
[11] H. R. Krishna-murthy, J. W. Wilkins, and K. G. Wilson, Phys. Rev. B **21**, 1003 (1980).
[12] H. R. Krishna-murthy, J. W. Wilkins, and K. G. Wilson, Phys. Rev. B **21**, 1044 (1980).
[13] S. Hershfield, J. H. Davies, and J. W. Wilkins, Phys. Rev. B **46**, 7046 (1992).
[14] A. Oguri, Phys. Rev. B **64**, 153305 (2001).
[15] C. Mora, Phys. Rev. B **80**, 125304 (2009).
[16] C. Mora, P. Vitushinsky, X. Leyronas, A. A. Clerk, and K. Le Hur, Phys. Rev. B **80**, 155322 (2009).
[17] C. Mora, C. P. Moca, J. von Delft, and G. Zaránd, Phys. Rev. B **92**, 075120 (2015).
[18] M. Filippone, C. P. Moca, A. Weichselbaum, J. von Delft, and C. Mora, Phys. Rev. B **98**, 075404 (2018).
[19] A. Oguri and A. C. Hewson, Phys. Rev. Lett. **120**, 126802 (2018).
[20] A. Oguri and A. C. Hewson, Phys. Rev. B **97**, 045406 (2018).
[21] A. Oguri and A. C. Hewson, Phys. Rev. B **97**, 035435 (2018).
[22] D. B. Karki and M. N. Kiselev, Phys. Rev. B **96**, 121403(R) (2017).
[23] D. B. Karki, C. Mora, J. von Delft, and M. N. Kiselev, Phys. Rev. B **97**, 195403 (2018).
[24] D. B. Karki and M. N. Kiselev, Phys. Rev. B **98**, 165443 (2018).
[25] C. P. Moca, C. Mora, I. Weymann, and G. Zaránd, Phys. Rev. Lett. **120**, 016803 (2018).
[26] Y. Teratani, R. Sakano, and A. Oguri, Phys. Rev. Lett. **125**, 216801 (2020).
[27] A. Oguri, Y. Teratani, K. Tsutsumi, and R. Sakano, Phys. Rev. B **105**, 115409 (2022).
[28] K. Tsutsumi, Y. Teratani, R. Sakano, and A. Oguri, Phys. Rev. B **104**, 235147 (2021).
[29] K. Tsutsumi, Y. Teratani, K. Motoyama, R. Sakano, and A. Oguri, Phys. Rev. B **108**, 045109 (2023).
[30] L. I. Glazman and M. E. Raikh, JETP Lett. **47**, 452 (1988).
[31] T. K. Ng and P. A. Lee, Phys. Rev. Lett. **61**, 1768 (1988).
[32] N. S. Wingreen and Y. Meir, Phys. Rev. B **49**, 11040 (1994).
[33] Y. Meir and N. S. Wingreen, Phys. Rev. Lett. **68**, 2512 (1992).
[34] W. Izumida, O. Sakai, and Y. Shimizu, Journal of the Physical Society of Japan **67**, 2444 (1998).
[35] W. Izumida, O. Sakai, and S. Suzuki, J. Phys. Soc. Jpn. **70**, 1045 (2001).
[36] A. A. Aligia, Journal of Physics: Condensed Matter **24**, 015306 (2012).
[37] A. A. Aligia, Phys. Rev. B **89**, 125405 (2014).

- [38] A. O. Gogolin and A. Komnik, *Phys. Rev. Lett.* **97**, 016602 (2006).
- [39] E. Sela, Y. Oreg, F. von Oppen, and J. Koch, *Phys. Rev. Lett.* **97**, 086601 (2006).
- [40] A. Golub, *Phys. Rev. B* **73**, 233310 (2006).
- [41] E. Sela and J. Malecki, *Phys. Rev. B* **80**, 233103 (2009).
- [42] R. Sakano, T. Fujii, and A. Oguri, *Phys. Rev. B* **83**, 075440 (2011).
- [43] T. A. Costi, A. C. Hewson, and V. Zlatić, *J. Phys.: Condens. Matter* **6**, 2519 (1994).
- [44] T. A. Costi, *Phys. Rev. B* **100**, 155126 (2019).
- [45] D. Goldhaber-Gordon, H. Shtrikman, D. Mahalu, D. Abusch-Magder, U. Meirav, and M. A. Kastner, *Nature* **391**, 156 (1998).
- [46] D. Goldhaber-Gordon, J. Göres, M. A. Kastner, H. Shtrikman, D. Mahalu, and U. Meirav, *Phys. Rev. Lett.* **81**, 5225 (1998).
- [47] S. M. Cronenwett, T. H. Oosterkamp, and L. P. Kouwenhoven, *Science* **281**, 540 (1998).
- [48] W. G. van der Wiel, S. D. Franceschi, T. Fujisawa, J. M. Elzerman, S. Tarucha, and L. P. Kouwenhoven, *Science* **289**, 2105 (2000).
- [49] I. V. Borzenets, J. Shim, J. C. H. Chen, A. Ludwig, A. D. Wieck, S. Tarucha, H.-S. Sim, and M. Yamamoto, *Nature* **579**, 210 (2020).
- [50] M. Grobis, I. G. Rau, R. M. Potok, H. Shtrikman, and D. Goldhaber-Gordon, *Phys. Rev. Lett.* **100**, 246601 (2008).
- [51] G. D. Scott, Z. K. Keane, J. W. Ciszek, J. M. Tour, and D. Natelson, *Phys. Rev. B* **79**, 165413 (2009).
- [52] O. Zarchin, M. Zaffalon, M. Heiblum, D. Mahalu, and V. Umansky, *Phys. Rev. B* **77**, 241303(R) (2008).
- [53] T. Delattre, C. Feuillet-Palma, L. G. Herrmann, P. Morfin, J.-M. Berroir, G. FShu ve, B. PlaXun ais, D. C. Glatthli, M.-S. Choi, C. Mora, and T. Kontos, *Nature Physics* **5**, 208 (2009).
- [54] Y. Yamauchi, K. Sekiguchi, K. Chida, T. Arakawa, S. Nakamura, K. Kobayashi, T. Ono, T. Fujii, and R. Sakano, *Phys. Rev. Lett.* **106**, 176601 (2011).
- [55] M. Ferrier, T. Arakawa, T. Hata, R. Fujiwara, R. Delagrè, R. Weil, R. Deblock, R. Sakano, A. Oguri, and K. Kobayashi, *Nat. Phys.* **12**, 230 (2016).
- [56] T. Hata, Y. Teratani, T. Arakawa, S. Lee, M. Ferrier, R. Deblock, R. Sakano, A. Oguri, and K. Kobayashi, *Nature Communications* **12**, 3233 (2021).
- [57] C. Hsu, T. A. Costi, D. Vogel, C. Wegeberg, M. Mayor, H. S. J. van der Zant, and P. Gehring, *Phys. Rev. Lett.* **128**, 147701 (2022).
- [58] A. Svilans, M. Josefsson, A. M. Burke, S. Fahlvik, C. Thelander, H. Linke, and M. Leijnse, *Phys. Rev. Lett.* **121**, 206801 (2018).
- [59] E. A. Laird, F. Kuemmeth, G. A. Steele, K. Grove-Rasmussen, J. Nygård, K. Flensberg, and L. P. Kouwenhoven, *Rev. Mod. Phys.* **87**, 703 (2015).
- [60] L. Borda, G. Zaránd, W. Hofstetter, B. I. Halperin, and J. von Delft, *Phys. Rev. Lett.* **90**, 026602 (2003).
- [61] M.-S. Choi, R. López, and R. Aguado, *Phys. Rev. Lett.* **95**, 067204 (2005).
- [62] M. Eto, *Journal of the Physical Society of Japan* **74**, 95 (2005).
- [63] R. Sakano and N. Kawakami, *Phys. Rev. B* **73**, 155332 (2006).
- [64] F. B. Anders, D. E. Logan, M. R. Galpin, and G. Finkelstein, *Phys. Rev. Lett.* **100**, 086809 (2008).
- [65] I. Weymann, R. Chirla, P. Trocha, and C. P. Moca, *Phys. Rev. B* **97**, 085404 (2018).
- [66] M. Filippone, C. P. Moca, G. Zaránd, and C. Mora, *Phys. Rev. B* **90**, 121406(R) (2014).
- [67] D. Mantelli, C. P. Moca, G. Zarand, and M. Grifoni, *Physica E: Low-dimensional Systems and Nanostructures* **77**, 180 (2016).
- [68] Y. Teratani, R. Sakano, T. Hata, T. Arakawa, M. Ferrier, K. Kobayashi, and A. Oguri, *Phys. Rev. B* **102**, 165106 (2020).
- [69] S. Sasaki, S. De Franceschi, J. M. Elzerman, W. G. van der Wiel, M. Eto, S. Tarucha, and L. P. Kouwenhoven, *Nature* **405**, 764 (2000).
- [70] P. Jarillo-Herrero, J. Kong, H. S. J. van der Zant, C. Dekker, L. P. Kouwenhoven, and S. De Franceschi, *Phys. Rev. Lett.* **94**, 156802 (2005).
- [71] B. Babić, T. Kontos, and C. Schönenberger, *Phys. Rev. B* **70**, 235419 (2004).
- [72] A. Makarovski, A. Zhukov, J. Liu, and G. Finkelstein, *Phys. Rev. B* **75**, 241407(R) (2007).
- [73] J. P. Cleuziou, N. V. N'Guyen, S. Florens, and W. Wernsdorfer, *Phys. Rev. Lett.* **111**, 136803 (2013).
- [74] T. Kuzmenko, K. Kikoin, and Y. Avishai, *Phys. Rev. B* **73**, 235310 (2006).
- [75] R. López, T. Rejec, J. Martinek, and R. Žitko, *Phys. Rev. B* **87**, 035135 (2013).
- [76] I. Kuzmenko and Y. Avishai, *Phys. Rev. B* **89**, 195110 (2014).
- [77] C. Caroli, R. Combescot, and P. Nozières, *Phys. C: Solid State Phys* **4**, 916 (1971).
- [78] S. Hershfield, *Phys. Rev. B* **46**, 7061 (1992).
- [79] G. D. Guttman, E. Ben-Jacob, and D. J. Bergman, *Phys. Rev. B* **51**, 17758 (1995).
- [80] T. A. Costi and V. Zlatić, *Phys. Rev. B* **81**, 235127 (2010).
- [81] R. Chirla and C. P. Moca, *Phys. Rev. B* **89**, 045132 (2014).
- [82] D. Pérez Daroca, P. Roura-Bas, and A. A. Aligia, *Phys. Rev. B* **97**, 165433 (2018).
- [83] A. C. Hewson, *J. Phys.: Condens. Matter* **13**, 10011 (2001).
- [84] A. C. Hewson, A. Oguri, and D. Meyer, *Eur. Phys. J. B* **40**, 177 (2004).
- [85] K. M. Stadler, A. K. Mitchell, J. von Delft, and A. Weichselbaum, *Phys. Rev. B* **93**, 235101 (2016).
- [86] W. C. Oliveira and L. N. Oliveira, *Phys. Rev. B* **49**, 11986 (1994).
- [87] Y. Nishikawa, D. J. G. Crow, and A. C. Hewson, *Phys. Rev. B* **82**, 115123 (2010).
- [88] Y. Nishikawa, D. J. G. Crow, and A. C. Hewson, *Phys. Rev. B* **82**, 245109 (2010).
- [89] A. Oguri, R. Sakano, and T. Fujii, *Phys. Rev. B* **84**, 113301 (2011).
- [90] A. Oguri, *Phys. Rev. B* **85**, 155404 (2012).